Escola de Camins
Escola Tècnica Superior d'Enginyeria de Camins, Canals i Ports
UPC BARCELONATECH

TREBALL FINAL DE MÀSTER

Orthogonal Subgrid Scale stabilization for nonlinear reaction-convection-diffusion equations

Treball realitzat per:
Sanjay Komala Sheshachala

Dirigit per:
Prof. Ramon Codina

Màster en:
Erasmus Mundus Computational Mechanics

Barcelona, 23 de juny de 2016

Departament d'enginyeria civil I ambiental

Orthogonal Subgrid Scale stabilization for nonlinear reaction-convection-diffusion equations

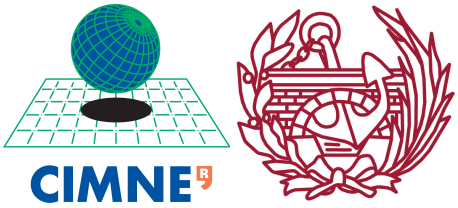

Sanjay Komala Sheshachala

Universitat Politècnica de Catalunya

Supervised by

Prof. Ramon Codina

A thesis submitted for the degree of

Master of Science in Computational Mechanics

2016

Dedicated to my parents

Acknowledgements

I would like to thank Prof. Codina for being a great teacher and taking me under his tutorship. Also I would like to convey my gratitude toward him for being helpful and approachable in all aspects during the thesis preparation. Many thanks to Arnau Pont for the help extended towards me.

It would be impossible for me to carry-out this project had it not been for the amazing teaching at both institutes, SwanseaUni and BarcelonaTech. A big shout-out to all my teachers for being truly inspirational. I gratefully acknowledge the Erasmus Mundus scholarship by the European Commission for making the master's study possible.

I am amazed and humbled by the never-ending love and support extended towards me from my family and friends. A heartfelt thanks to all, I feel blessed to have them in my life.

Abstract

Nonlinear reaction-convection-diffusion equations are encountered in modeling of a variety of natural phenomena such as in chemical reactions, population dynamics and contaminant dispersal. When the scale of convective and reactive phenomena are large, Galerkin finite element solution fails.

As a remedy, Orthogonal Subgrid Scale stabilization is applied to the finite element formulation. It has its origins in the Variational Multi Scale approach. It is based on a fine grid - coarse grid component sum decomposition of solution and utilizes the fine grid solution orthogonal to the residual of the finite element coarse grid solution as a correction term. With selective mesh refinement, a stabilized oscillation-free solution that can capture sharp layers is obtained. Newton Raphson method is utilized for the linearization of nonlinear reaction terms. Backward difference scheme is used for time integration.

The formulation is tested for cases with standalone and coupled systems of transient nonlinear reaction-convection-diffusion equations. Method of manufactured solution is used to test for correctness and bug-free implementation of the formulation. In the error analysis, optimal convergence is achieved. Applications in channel flow, cavity flow and predator-prey model is used to highlight the need and effectiveness of the stabilization technique.

Keywords. finite element, stabilization, Variational Multi Scale, nonlinear reaction, predator-prey

Contents

List of Figures

Nomenclature

Roman Symbols

$\bar{u}$	Coarse grid solution
$\mathbf{a}$	Convective velocity
$\mathbf{f}$	Finite element source vector
$\mathbf{K}$	Finite element assembled matrix
$\mathbf{M}$	Finite element mass matrix
$\mathbf{r}$	Finite element residual
$\mathbf{T}$	Tangent stiffness matrix
$\mathbf{u}$	Finite element solution vector
$\tilde{u}$	Fine grid solution
B	Predator-prey: Predation rate
E	Predator-prey: Predation function
f	Source/sink
H	Predator-prey: Half saturation prey density
h	characteristic mesh size
k	Coefficient of diffusion

P Predator-prey: Prey population growth function

s Coefficient of reaction

u Quantity of interest

Da Damköhler number

Pe Peclet number

Re Reynold's number

Greek Symbols

κ Predator-prey: Predation efficiency

μ Predator-prey: Predator mortality function

τ Stabilization parameter

Superscripts

$\perp$ Orthogonal component

n Time step index

Subscripts

h Finite element space

i Newton Raphson interation counter

Acronyms

BDF1 Backward Difference Formula of 1^{st} order

BDF2 Backward Difference Formula of 2^{nd} order

CDRE Convection-Diffusion-Reaction Equation

OSS Orthogonal Subgrid Scale method

VMS Variational Multi Scale method

Chapter 1

Introduction

Many processes in nature are modelled as a combination of diffusive, advective and reactive phenomena. One can come across Convection-Diffusion-Reaction Equations (CDRE) models in varied fields in science. Population dynamics models to describe the proliferation of living organisms Fisher [1937], predator-prey models Holzer [2014] Hamidi et al. [2012] Cussler [2013], heat and mass transfer models Danilov et al. [2012], chemical reaction models Cussler [2013] and chemotaxis models Zhang et al. [2016] incorporate convection, diffusion or reaction terms. In this chapter we take a close look at the various applications of CDRE to model different physical phenomenon. Obstacles encountered while solving the CDRE numerically are laid out and a motivation to adopt the proposed stabilization method for finite element solution of CDRE equation is presented.

1.1 CDR models in nature

Evolution of many entities may involve a combination of spreading (diffusion), bulk movement (convection), creation or destruction (reaction) phenomena. Mathematically, they can be described by diffusion, convection and reaction operators acting on the quantity of interest. Such descriptions result in models that describe a wide variety of phenomena which can be mathematically analyzed and solved for.

We can encounter models in biology to study population of organisms Fisher

[1937] and propagation of nerve pulses in a neuron Nagumo et al. [1962]. In chemistry, they are used to model chemical reactions Cussler [2013]. Models for circuit theory in electronic design Linares-Barranco et al. [1991], rumor spreading in sociology Zhu et al. [2016] demonstrate the prevalence and ubiquity of CDRE.

1.1.1 General form of CDRE

Let us denote the quantity of interest of the CDRE by u which is a scalar in our case (it could also be a vector $\mathbf{u}$). The quantity of interest may describe population density, concentration of chemical species, etc. The general form of the CDRE consist of five terms:

1. The diffusion term signifies the spreading of the species in space. Physics dictates that transport of quantity of interest u occurs from a region of higher concentration to a region of lower concentration. Hence quantity u diffuses/spreads out from a region of high concentration. This process is modelled by the laplacian operator. Laplacian is given by the divergence of gradient operator ($\Delta u = \nabla \cdot \nabla u$). In physics, we come across phenomenon where the diffusion is generally given by $\nabla \cdot k\nabla u$, where k is called the coefficient of diffusion. k can be a constant or a function of space and time.

2. The convection term signifies the bulk movement of species in space and time. Matter gets transported in the domain at a velocity called convective/advective velocity. It is denoted by $\mathbf{a}$. Such phenomena is common for fluid mechanics problems with heat and/or mass transfer. The advection term is given by the dot product of gradient of u and the convective velocity velocity ($\mathbf{a}\cdot\nabla u$). Advective velocity can be a constant or a function of space and time.

3. The reaction term models the creation or destruction of the quantity of interest in space and time. In chemical processes, it can signify the creation of new products and consumption of reactants. In population studies, it signifies the birth and mortality of species. Reaction term is given by su, where s is the reaction coefficient. s can be a constant or a function of space and time. Also the reaction term is nonlinear if s is a function of u.

4. Temporal derivative term is present if the quantity of interest u varies in time. But if only a steady state solution is expected, this term is neglected. Temporal derivative is given by $\partial_t u = \dfrac{\partial u}{\partial t}$

5. Source term is used to add or subtract the quantity of interest into the domain of interest. It is denoted by f. It can be constant or a function of space and time.

The problem is now to find the quantity of interest u in the domain of interest Ω, such that the initial and boundary conditions are satisfied. It can be stated as:

$$\begin{aligned}
&\text{Find } u \text{ such that} \\
\partial_t u - k\Delta u + \mathbf{a}\cdot\nabla u + su = \quad & f \quad \text{in} \quad \Omega, t > 0 && (1.1)\\
\text{Initial condition: } u = \quad & u_0 \quad \text{in} \quad \Omega, t = 0 && (1.2)\\
\text{Dirichlet boundary condition: } u = \quad & u_D \quad \text{on} \quad \partial\Omega_D, t > 0 && (1.3)\\
\text{Neumann boundary condition: } k\,\mathbf{n}\cdot\nabla u = \quad & u_N \quad \text{on} \quad \partial\Omega_N, t > 0 && (1.4)
\end{aligned}$$

In the present study we consider nonlinearity only in the reaction term. Hence, we explore solutions to CDRE where $s = s(u)$

1.1.2 CDRE with nonlinear reaction terms

Models that involve diffusion and nonlinear reaction terms of the quantity of interest u are generally presented in literature in the following form:

$$\begin{aligned}
\frac{Du}{Dt} &= k\Delta u + s(u) && (1.5)\\
\partial_t u + \mathbf{a}\cdot u &= k\Delta u + s(u) && (1.6)
\end{aligned}$$

where $s(u)$ is the nonlinear reaction term. A positive value of this term signifies generation and a negative value signifies destruction of u. Diffusion-reaction equations are generally solved for without a specified advection field. These forms of equations are encountered in population dynamics Fisher [1937] Tikhomirov [1991], pollution dispersal models and nonuniform chemical reaction models Cus-

sler [2013]. Such equations generally exhibit traveling wave solutions and formation of spacio-temporal patterns in solution Volpert and Petrovskii [2009] Pao [1982]. Turing patterns Turing [1952] and patterns in Belousov-Zabotinski reactions Zhang et al. [1993] are some such examples. In our study, we explore solution with added advection field, since its addition is one of the challenges in obtaining numerical solutions.

One of the most popular model for nonlinear reaction term is the Fisher-KPP model. Fisher Fisher [1937] and the team of Kolmogorov, Petrovsky and Piskunov Tikhomirov [1991] arrived at Eqn 1.7 independently to model the population density of species in ecology. It has since been extended to various other application domains. Fisher-KPP equation is given below:

$$\partial_t u + \mathbf{a} \cdot \nabla u \quad = k\Delta u + s(1 - \frac{u}{K})u \tag{1.7}$$

Convective velocity $\mathbf{a}$ and reactive coefficient s are constants. The reaction term is the so-called logistic term. K denotes the maximum carrying capacity of the system for the species u. Hence Eqn 1.7 models dispersion of species subjected to the carrying capacity of the system and given convective velocity (advection is used to model migration towards food sources or safety). This equation exhibits a single traveling wave front solution.

Another important equation in study of nonlinear reaction-diffusion models is the Nagumo equation. It has been used to model propagation of nerve impulses, in circuit theory for electronics and propagation of flames Aronson and Weinberger [1975]. It reads:

$$\partial_t u + \mathbf{a} \cdot \nabla u \quad = k\Delta u + s(a - u)(u - b)u \tag{1.8}$$

where a and b are constants. Several notable extensions to Fisher KPP equation are available. Fitzhugh - Nagumo equations is a system of equation for propagation of waves through excitable media Nagumo et al. [1962], Barkley model for catalytic reactions Bär and Eiswirth [1993] and Gross-Pitaevski equation to describe Bose Einstein condensates in quantum mechanics Gross [1961].

Extensive study have been carried out to obtain conditions for well-posedness

of the Fisher-KPP equation. Conditions for the existence of solution, bifurcation phenomena are well explored Volpert and Petrovskii [2009].

Several studies have been conducted to apply numerical methods to solve CDRE, most of them are restricted to generic 1D problems Tang and Weber [1991]. Analytical solutions have been explored for simple problems too Magyari [2008]. One of the important themes of the present work is to explore the application of finite element method with stabilization to solve the nonlinear CDRE in 2D. Hence for our efforts, we develop the solution for Fisher KPP equation. Also population models with different types of nonlinear reaction term are solved in the predator-prey modeling at the end of this thesis.

1.2 Solution of CDRE with finite elements

Non-dimensional numbers of great significance for finite element solution of CDR equations are the numerical Peclet number and mesh dependent Damköhler number defined below:

$$\text{Numerical Pèclet number} = \quad Pe = \frac{|\mathbf{a}|h}{2k} \tag{1.9}$$

$$\text{Numerical Damköler number} = \quad Da = \frac{sh^2}{k} \tag{1.10}$$

where h represents the characteristic size of the finite element discretization.

Numerical Peclet number Pe, is a measure of the relative strength of convection to that of diffusion. Mesh dependent Damköhler number Da, is a measure of relative strength of reaction to that of diffusion.

Standard Galerkin finite elements fail when $Pe > 1$ or when $Da >> 1$.

Our proposed remedy is to add stabilization to the Galerkin finite element method. This thesis explores the approach of Orthogonal Subgrid Scale (OSS) stabilization Codina [2002] which in turn is based on Variational Multi Scale methods (VMS) proposed by Hughes Hughes [1995].

1.3 Outline of the thesis

In the present work, we begin with presenting the formulation and implementation of the Orthogonal Subgrid Scale method for a linear CDRE. This is then later extended to nonlinear CDRE, time-dependent/transient nonlinear CDRE and finally to a system of coupled, transient, nonlinear CDRE. Newton Raphson method used for linearization of nonlinear equation is explained. Backward difference scheme used for time integration is detailed. The accuracy of solution obtained from these implementations are then tested with method of manufactured solutions for convergence. Further, examples of channel flow, cavity flow and predator-prey modelling is presented to highlight the effectiveness of the stabilization method.

Chapter 2

Orthogonal Subgrid Scale stabilization

In this chapter, we discuss the origins of Orthogonal Subgrid Scale stabilization in the Variational Multi Scale method. A formulation suited for linear CDRE is presented and the implementation procedure is detailed. Since we only deal with nonlinearity in the reaction term, the linearization procedure introduced in the next section will not affect the OSS stabilization term. Moreover we do not let subgrid scale term vary in time. Thus the time integration discussed in the next chapter does not affect the OSS stabilization term too. (See Codina and Blasco [2002] for time dependent subgrid scales and how they need to be tracked at each time step for more details)

2.1 Introduction to Subgrid Scales

Most prevalent phenomena in physical sciences are multi-scale in nature. Galerkin finite element solution to partial differential equations arising from such models suffer from inaccuracy. Classical case of solution to convection dominated flow problems with Galerkin finite element lead to oscillatory solution. Several stabilization techniques were introduced to attenuate the problem. This led the extension of Galerkin finite element into Galerkin Least Squares, Stabilized Upwind Petrov Galerkin (SUPG), Taylor Galerkin etc.

The seminal work by Hughes et. al. in 1995 Hughes [1995] on Variational Multi Scale formulation brought all the stabilization techniques under a common umbrella with a single theoretical framework. It introduced the concept of subgrid scale model. Each of the stabilization techniques that had appeared earlier in literature was shown to arise from a particular class of subgrid scale models as suggested by Hughes Hughes et al. [1998] and was elucidated by Codina Codina [1998]. This abstraction led to further development of stabilization methods Hughes et al. [1998].

The basic idea of VMS approach is that the solution u can be evaluated as the sum of the two components $u = \bar{u} + \tilde{u}$. $\bar{u}$ is the so-called coarse grid solution which is typically solved numerically using finite element method. And $\tilde{u}$ is the so-called fine grid solution which is determined analytically a priori. The idea is to obtain the 'effect' of $\tilde{u}$ on $\bar{u}$ rather than an explicit expression for $\tilde{u}$. $\tilde{u}$ affects the solution globally but when it is defined, it may be done so locally or globally. The effect of $\bar{u}$ is always global Hughes et al. [1998]. The end result is an additional term to the Galerkin finite element formulation.

Therefore, a good design of the fine grid solution is the logical next step. The relationship between the coarse grid and the fine grid component plays a major role in this process. Let the finite dimension space of coarse grid solution be $\bar{V}$. The fine grid solution can be chosen from an infinite dimension subspace $\tilde{V}$ of the solution space V such that $V = \tilde{V} \oplus \bar{V}$. Now if our formulation is exact, we obtain that the fine grid solution must be the error in the coarse grid solution Hughes et al. [1998].

2.2 OSS formulation for a stationary, linear CDRE

In this section we consider a stationary linear CDRE with $k > 0$, $s \geq 0$ and constant velocity $\mathbf{a} \in \mathbb{R}^d$ where $d = (2, 3)$ is the dimension of the problem. We shall elucidate the development of the OSS formulation resulting in the final equation containing the Galerkin formulation term and an additional stabilization term which provides control over and suppress the oscillations in the finite element solution.

We solve the following stationary CDRE subjected to the homogeneous Dirich-

let boundary condition:

$$\text{Find } u \text{ such that}$$

$$\mathcal{L}u := -k\Delta u + \mathbf{a} \cdot \nabla u + su = \quad f \quad \text{in } \Omega \tag{2.1}$$

$$u = \quad 0 \quad \text{on } \partial\Omega \tag{2.2}$$

Using the test function $v \in V$ the weak form of the equation is obtained. Here the solution space $V = H_0^1(\Omega)$. We define the space $H_0^1(\Omega) = \{u | u \in L^2(\Omega), \nabla u \in L^2(\Omega) \text{ and } u = 0 \text{ on } \partial\Omega\}$. The problem is to find $u \in V$ such that the following holds

$$B(v, u) := k(\nabla v, \nabla u) + (v, \mathbf{a} \cdot \nabla u) + s(v, u) = \quad \langle v, f \rangle \quad \forall v \in V \tag{2.3}$$

where $(\cdot, \cdot)$ is the L^2 inner product and $\langle \cdot, \cdot \rangle$ is the integral of product of two functions.

When finite element solution is sought, the solution space is $V_h \subset V$ which is built from a partition $\mathcal{P} = \{J\}$ of the domain Ω (meshing with J elements). Using conformal Galerkin finite element formulation, now the problem is as follows

$$\text{Find } u_h \in V_h \text{ such that}$$

$$B(v_h, u_h) = \quad \langle v_h, f \rangle \quad \forall v_h \in V_h \tag{2.4}$$

Introducing the subgrid scale into the formulation, we decompose the solution u into the component solved by finite element approximation u_h and the unresolvable component $\tilde{u}$. As a result, the solution space now is $V = V_h \oplus \tilde{V}$. Two equations arise from testing the weak form with test functions v_h and $\tilde{v}$.

$$B(u_h, v_h) + B(\tilde{u}, v_h) = \quad \langle f, v_h \rangle \quad \forall v_h \in V_h \tag{2.5}$$

$$B(u_h, \tilde{v}) + B(\tilde{u}, \tilde{v}) = \quad \langle f, \tilde{v} \rangle \quad \forall \tilde{v} \in \tilde{V} \tag{2.6}$$

Using the definition of inverse adjoint operator $\mathcal{L}^*$ and $B(u, v) = \langle \mathcal{L}u, v \rangle$, the

equations become

$$B(u_h, v_h) + \langle \tilde{u}, \mathcal{L}^* v_h \rangle = \langle f, v_h \rangle \quad \forall v_h \in V_h \tag{2.7}$$

$$\langle \mathcal{L} u_h, \tilde{v} \rangle + \langle \mathcal{L}\tilde{u}, \tilde{v} \rangle = \langle f, \tilde{v} \rangle \quad \forall \tilde{v} \in \tilde{V} \tag{2.8}$$

We introduce two approximations to the subgrid scale component $\tilde{u}$. Firstly, we suppose that the jumps of the solution derivatives across the element boundaries are zero. But this in not a necessary condition as shown in the reference Baiges [2009]. The article indicates that the choice of subgrid scale must be able to satisfy the condition that the value of subgrid scales at the boundary should be proportional to the jump of the flux of finite element component and the average of the subgrid scale value in the element interior. With our approximation, we have:

$$\langle \mathcal{L} u_h, \tilde{v} \rangle \approx \sum_J (\mathcal{L} u_h, \tilde{v}) \equiv (\mathcal{L} u_h, \tilde{v})_h \tag{2.9}$$

Second approximation is as follows:

$$\langle \mathcal{L}\tilde{u}, \tilde{v} \rangle = \tau^{-1}(\tilde{u}, \tilde{v}) \tag{2.10}$$

where τ is called the stabilization parameter and is defined in Eqn 2.11. For the given problem with zero Dirichlet boundary condition, the maximum principle for a continuous problem ensures that the solution attains its maximum value along the boundary when the source term is negative. This property needs to be carried into the discrete form of the equation. The value of the coefficients defining τ are obtained from the article Codina [1998] and are shown below. The article Codina [2010] provides an in-depth treatment on the stabilization parameter. τ is defined as:

$$\tau^{-1} = c_1 \frac{k}{h^2} + c_2 \frac{|\mathbf{a}|}{h} + c_3 s \tag{2.11}$$

where c_1, c_2 and c_3 are constants. For linear finite elements:

$$\tau^{-1} = \frac{4k}{h^2} + \frac{2|\mathbf{a}|}{h} + s \tag{2.12}$$

The equations now become

$$B(u_h, v_h) + (\tilde{u}, \mathcal{L}^* v_h)_h = \langle f, v_h \rangle \quad \forall v_h \in V_h \tag{2.13}$$

$$\langle \mathcal{L} u_h, \tilde{v} \rangle + \tau^{-1}(\tilde{u}, \tilde{v}) = \langle f, \tilde{v} \rangle \quad \forall \tilde{v} \in \tilde{V} \tag{2.14}$$

The subgrid space is yet to be defined and it may not belong to $H_0^1(\Omega)$. We consider that the subgrid solution is comprised of the L^2 projection onto the space $\tilde{V}$ (denoted by $\tilde{P}$) of the residual of finite element solution.

$$\tilde{u} = \tau \tilde{P}(f - \mathcal{L} u_h) \tag{2.15}$$

In Orthogonal Subgrid Scale stabilization, the subgrid space is orthogonal to the finite element space V_h. Hence we take into account only the orthogonal component of the projection

$$\tilde{V} = V_h^{\perp} \tag{2.16}$$

$$\tilde{u} = \tau P_h^{\perp}(f - \mathcal{L} u_h) \tag{2.17}$$

A further simplification is to consider the convective component of the residual alone. This is because Galerkin formulation precisely lacks control over the convective term $(\mathbf{a} \cdot \nabla u_h)$ and addition of this term to the orthogonal component adds stability to the formulation. This is in contrast to the algebraic subgrid scale choice, $\tilde{u} = \tau(f - \mathcal{L} u_h)$ which adds components that lead to stable but 'over-diffusive' solution. Thus, we may take

$$\tilde{u} = -\tau P_h^{\perp}(\mathbf{a} \cdot \nabla u_h) \tag{2.18}$$

Substituting this value in Eqn. 2.13

$$B(u_h, v_h) + (-\tau P_h^{\perp}(\mathbf{a} \cdot \nabla u_h), \mathcal{L}^* v_h)_h = \langle f, v_h \rangle \quad \forall v_h \in V_h \tag{2.19}$$

We can simplify above expression by using the value of adjoint operator and the property of L^2 norm with an orthogonally projected component

$$\mathcal{L}^* v_h = \overbrace{-k\Delta v_h}^{=0} - \mathbf{a}\cdot\nabla v_h + s v_h \tag{2.20}$$

$$P^{\perp}(s v_h) = 0 \tag{2.21}$$

$$(P_h^{\perp}(\mathbf{a}\cdot\nabla u_h), (\mathbf{a}\cdot\nabla v_h)) = (P_h^{\perp}(\mathbf{a}\cdot\nabla u_h), P_h^{\perp}(\mathbf{a}\cdot\nabla v_h)) \tag{2.22}$$

Hence the final equation with the additional orthogonal term is given below

$$B(u_h, v_h) + \tau(P_h^{\perp}(\mathbf{a}\cdot\nabla u_h), P_h^{\perp}(\mathbf{a}\cdot\nabla v_h))_h = \langle f, v_h\rangle \quad \forall v \in V_h \tag{2.23}$$

In the next section, we discuss the finite element implementation of equation 2.23

Remark. *Orthogonal Subgrid Scale provides global bounds for the solution, not locally since the method lacks monotonicity. Hence only global convergence is guaranteed. Typically oscillations are restricted to only a few layers. This is easily mitigated by using shock-capturing techniques or selective mesh refinement*

2.3 Implementation of OSS stabilization

In this section, we describe the term-by-term implementation of the Eqn 2.23 to show its algebraic form.

2.3.1 FEM terms

The implementation of the Galerkin finite element terms is using the first order approximation. The solution is approximated as a combination of shape functions $N^a(x)$ and nodal values u^a as shown below.

$$u_h = \sum_a^n u^a N^a(x) \tag{2.24}$$

$$v_h = \sum_b^n v^b N^b(x) \tag{2.25}$$

where superscript n is the number of degrees of freedom.

Hence the term $B(u_h, v_h)$ becomes

$$\begin{aligned} B(u_h, v_h) = \quad & k\Big(\textstyle\sum_b^n v^b \nabla N^b(x), \sum_a^n u^a \nabla N^a(x) \Big) \\ & + \Big(\textstyle\sum_b^n v^b N^b(x), \sum_a^n u^a \mathbf{a} \cdot \nabla N^a(x) \Big) \\ & + s\Big(\textstyle\sum_b^n v^b N^b(x), \sum_a^n u^a N^a(x) \Big) \end{aligned} \tag{2.26}$$

Defining diffusion, convection and reaction matrices as

$$\mathbf{K}_k|_{ab} = k \textstyle\int_\Omega \nabla N^b(x) \cdot \nabla N^a(x) \tag{2.27}$$

$$\mathbf{K}_a|_{ab} = \textstyle\int_\Omega N^b(x)(\mathbf{a} \cdot \nabla N(x)^a) \tag{2.28}$$

$$\mathbf{K}_s|_{ab} = s \textstyle\int_\Omega N^b(x) N^a(x) \tag{2.29}$$

we obtain

$$B(u_h, v_h) = \mathbf{v}^T(\mathbf{K}_k + \mathbf{K}_a + \mathbf{K}_s)\mathbf{u} \tag{2.30}$$

$\mathbf{u}$ is the vector of unknowns

The source term is computed as

$$\langle f, v_h \rangle = \langle f, \sum_b^n v_h^b N^b(x) \rangle = \mathbf{v}^T \mathbf{f} \quad \forall v_h \in V_h \tag{2.31}$$

where

$$\mathbf{f}|_j = \int_\Omega f N^b(x) \tag{2.32}$$

2.3.2 OSS stabilzation term

The L^2 projection of the finite element convection term is obtained from the property for projections that dictates the following:

$$\Big(P_h(\mathbf{a} \cdot \nabla u_h), v_h \Big) = \Big((\mathbf{a} \cdot \nabla u_h), v_h \Big) \quad \forall v_h \in V_h \tag{2.33}$$

Approximating $P_h(\mathbf{a}\cdot\nabla u_h) = \sum_a r^a N^a(x)$, we substitute in Eqn. 2.33

$$\int_\Omega \sum_a r^a N^a(x) \sum_b v_h^b N^b(x) = \int_\Omega \sum_a u_h^a (\mathbf{a}\cdot\nabla N^a(x)) \sum_b v_h^b N^b(x) \tag{2.34}$$

$$\tag{2.35}$$

Defining the matrices as follows,

$$\mathbf{M}|_{ab} = \int_\Omega N^b(x) N^a(x) \tag{2.36}$$

$$\mathbf{L}|_{ab} = \int_\Omega N^b(x) (\mathbf{a}\cdot\nabla N(x))^a \tag{2.37}$$

we obtain the solution in algebraic form where $\mathbf{r}$ is the vector of unknowns.

$$\mathbf{Mr} = \mathbf{Lu} \tag{2.38}$$

$$\mathbf{r} = \mathbf{M^{-1}Lu} \tag{2.39}$$

The orthogonal component of projection is obtained with the following relation:

$$P_h^\perp(\mathbf{a}\cdot\nabla u_h) = \mathbf{a}\cdot\nabla u_h - P_h(\mathbf{a}\cdot\nabla u_h) \tag{2.40}$$

We use them in the final expression of the stabilization term. The algebraic

form of the scalar stabilization term $\tau(P_h^{\perp}(\mathbf{a}\cdot\nabla u_h), P_h^{\perp}(\mathbf{a}\cdot\nabla v_h))_h$ is given below

$$\text{Algebraic form:} \tag{2.41}$$

$$= \quad \tau \int_\Omega \Big(\Big([\textstyle\sum_c \mathbf{a}\cdot\nabla N^c]^T \mathbf{v} - [\sum_c N^c]^T \mathbf{M^{-1}L v} \Big)^T \tag{2.42}$$

$$\Big([\textstyle\sum_c \mathbf{a}\cdot\nabla N^c]^T \mathbf{u} - [\sum_c N^c]^T \mathbf{M^{-1}L u} \Big) \Big) \tag{2.43}$$

$$= \quad \tau \Big(\int_\Omega (\mathbf{a}\cdot\nabla N^i(x))(\mathbf{a}\cdot\nabla N^j(x)) \Big) \mathbf{u} \tag{2.44}$$

$$-\tau \Big(\int_\Omega (\mathbf{a}\cdot\nabla N^i(x))(\nabla N^j(x)) \Big) \mathbf{M^{-1}L u} \tag{2.45}$$

$$-\tau \mathbf{M^{-1}L} \Big(\int_\Omega (\nabla N^i(x))(\mathbf{a}\cdot\nabla N^j(x)) \Big) \mathbf{u} \tag{2.46}$$

$$+\tau \mathbf{M^{-1}L} \Big(\int_\Omega (\nabla N^i(x))(\nabla N^j(x)) \Big) \mathbf{M^{-1}L u} \tag{2.47}$$

$$= \quad \mathbf{K}_{OSS}\mathbf{u} \tag{2.48}$$

Collecting all the terms in Eqn 2.30 2.48 and 2.32 leads to the final algebraic system of equation

$$(\mathbf{K}_k + \mathbf{K}_a + \mathbf{K}_s + \mathbf{K}_{OSS})\mathbf{u} = \mathbf{f} \tag{2.49}$$

Chapter 3

Numerical Approximation

This chapter is devoted to the algorithms for numerical approximation for two cases, one for linearization of nonlinear reaction terms and the other for the time integration. We employ Newton Raphson iterative algorithm for linearization. And Backward Difference formula, particularly BDF2 is used for time integration.

3.1 Newton Raphson linearization

In this section we perform the linearization of the nonlinear stationary CDRE using Newton Raphson technique. Consider the nonlinear system as shown in Eqn 3.1.

$$\Big(\mathbf{K}_k + \mathbf{K}_a + \mathbf{K}_s(\mathbf{u}) + \mathbf{K}_{OSS}\Big)\mathbf{u} = \quad \mathbf{f} \tag{3.1}$$

where only the reaction matrix $\mathbf{K}_s(\mathbf{u})$ is a function of $\mathbf{u}$. Newton Raphson algorithm consists of performing iterations (update $\mathbf{u}_{i+1}$ using $\mathbf{u}_i$) until convergence starting with an initial solution $\mathbf{u}_0$ using Eqn 3.2.

$$\mathbf{u}_{i+1} = \mathbf{u}_i - \mathbf{T}^{-1}(\mathbf{u}_i)\mathbf{r}(\mathbf{u}_i) \tag{3.2}$$

$\mathbf{T}(\mathbf{u})$ is called the tangent stiffness matrix and $\mathbf{r}(\mathbf{u})$ is the residual, defined as

follows:

$$\mathbf{r}(\mathbf{u}) = \Big(\mathbf{K}_k + \mathbf{K}_a + \mathbf{K}_s(\mathbf{u}) + \mathbf{K}_{OSS}\Big)\mathbf{u} - \mathbf{f} \tag{3.3}$$

$$\mathbf{T}(\mathbf{u}) = \frac{d\mathbf{r}(\mathbf{u})}{d\mathbf{u}} = \mathbf{K}_k + \mathbf{K}_a + \mathbf{K}_s(\mathbf{u}) + \frac{d\mathbf{K}_s(\mathbf{u})}{d\mathbf{u}}\mathbf{u} + \mathbf{K}_{OSS} \tag{3.4}$$

The derivative is computed as shown below, where n is number of degrees of freedom

$$\Big(\frac{d\mathbf{K}_s(\mathbf{u})}{d\mathbf{u}}\mathbf{u}\Big)|_{ij} = \sum_{m=1}^{n} \frac{\partial \mathbf{K}_s(\mathbf{u})|_{im}}{\partial \mathbf{u}_j}\mathbf{u}_m \tag{3.5}$$

Finally we compute the tangent stiffness matrix at $\mathbf{u}_i$ using

$$\mathbf{T}(\mathbf{u}_i) = \mathbf{K}_k + \mathbf{K}_a + \mathbf{K}_s(\mathbf{u}_i) + \frac{d\mathbf{K}_s(\mathbf{u})}{d\mathbf{u}}|_{\mathbf{u}_i} + \mathbf{K}_{OSS} \tag{3.6}$$

to obtain the updated solution $\mathbf{u}_{i+1}$. This process is continued until the L^2 norm of the difference between two successive solutions (normalized) is less than the tolerance. In all cases presented in the next chapter, we set the tolerance to 10^{-4}.

3.2 BDF time integration

For a transient nonlinear CDRE, the total time is split into into intervals. At each time step the Newton Raphson linearization is to be performed. Consider the time dependent nonlinear CDR equation shown below in its differential and algebraic forms.

$$\partial_t u - k\Delta u + \mathbf{a} \cdot \nabla u + s(u)u = f \tag{3.7}$$

$$\mathbf{M}\frac{\partial u}{\partial t} + (\mathbf{K}_k + \mathbf{K}_a + \mathbf{K}_s(\mathbf{u}) + \mathbf{K}_{OSS})\mathbf{u} = \mathbf{f} \tag{3.8}$$

The Backward Difference scheme for time integration is given as follows

$$\text{BDF1:} \quad \frac{\partial u}{\partial t} = \frac{u^{n+1} - u^n}{\delta t} \quad \text{is } O(\delta t) \tag{3.9}$$

$$\text{BDF2:} \quad \frac{\partial u}{\partial t} = \frac{\frac{3}{2}u^{n+1} - 2u^n + \frac{1}{2}u^{n-1}}{\delta t} \quad \text{is } O(\delta t^2) \tag{3.10}$$

Using BDF1 and BDF2 in the transient equation, we obtain

$$(\frac{\mathbf{M}}{\delta t} + \mathbf{K}_k + \mathbf{K}_a + \mathbf{K}_s(\mathbf{u}^{n+1}) + \mathbf{K}_{OSS})\mathbf{u}^{n+1} = \mathbf{f} + \frac{\mathbf{M}}{\delta t}\mathbf{u}^n \tag{3.11}$$

$$(\frac{3}{2}\frac{\mathbf{M}}{\delta t} + \mathbf{K}_k + \mathbf{K}_a + \mathbf{K}_s(\mathbf{u}^{n+1}) + \mathbf{K}_{OSS})\mathbf{u}^{n+1} = \mathbf{f} + 2\frac{\mathbf{M}}{\delta t}\mathbf{u}^n - \frac{1}{2}\frac{\mathbf{M}}{\delta t}\mathbf{u}^{n-1} \tag{3.12}$$

The first time step cannot be solved with BDF2 since $\mathbf{u}^{n-1}$ is non-existent. Hence BDF1 is used for the first time step and the successive time integrations are carried out using BDF2.

When Newton Raphson linearization is applied, we obtain additional terms in the definition of Tangent stiffness matrix and the residual.

$$\mathbf{u}_{i+1}^{n+1} = \mathbf{u}_{i+1}^{n+1} - \mathbf{T}^{-\mathbf{1}}(\mathbf{u}_i^{n+1})\mathbf{r}(\mathbf{u}_i^{n+1}) \tag{3.13}$$

For the first time step using BDF1,

$$\mathbf{r}(\mathbf{u}^{n+1}) = (\frac{\mathbf{M}}{\delta t} + \mathbf{K}_k + \mathbf{K}_a + \mathbf{K}_s(\mathbf{u}^{n+1}) + \mathbf{K}_{OSS})\mathbf{u}^{n+1} - \frac{\mathbf{M}}{\delta t}\mathbf{u}^n - \mathbf{f} \tag{3.14}$$

$$\mathbf{T}(\mathbf{u}^{n+1}) = \frac{\mathbf{M}}{\delta t} + \mathbf{K}_k + \mathbf{K}_a + \mathbf{K}_s(\mathbf{u}^{n+1}) + \frac{d\mathbf{K}_s(\mathbf{u}^{n+1})}{d\mathbf{u}}\mathbf{u}^{n+1} + \mathbf{K}_{OSS} \tag{3.15}$$

For successive time steps using BDF2,

$$\mathbf{r}(\mathbf{u}^{n+1}) = (\frac{3}{2}\frac{\mathbf{M}}{\delta t} + \mathbf{K}_k + \mathbf{K}_a + \mathbf{K}_s(\mathbf{u}^{n+1}) + \mathbf{K}_{OSS})\mathbf{u}^{n+1} - 2\frac{\mathbf{M}}{\delta t}\mathbf{u}^n + \frac{1}{2}\frac{\mathbf{M}}{\delta t}\mathbf{u}^{n-1} - \mathbf{f} \tag{3.16}$$

$$\mathbf{T}(\mathbf{u}^{n+1}) = \frac{3}{2}\frac{\mathbf{M}}{\delta t} + \mathbf{K}_k + \mathbf{K}_a + \mathbf{K}_s(\mathbf{u}^{n+1}) + \frac{d\mathbf{K}_s(\mathbf{u}^{n+1})}{d\mathbf{u}}\mathbf{u}^{n+1} + \mathbf{K}_{OSS} \quad (3.17)$$

The new definitions of Tangent Siffness and residual can be used as discussed in previous section for the Newton Raphson iteration. Algorithm 1 gives the implementation of time integration (counter n) with Newton Raphson linearization (counter i).

Algorithm 1: Time integration with Newton Raphson Linearization

Data: $\mathbf{u}^n$, $\mathbf{u}^{n-1}$
while $n \neq$ *(end time)* **do**
  $i = 0$
  Initialize: $\mathbf{u}_i^{n+1} = \mathbf{u}^n$
  Initialize: $\mathbf{u}_i^{n} = \mathbf{u}^n$
  Initialize: $\mathbf{u}_i^{n-1} = \mathbf{u}^{n-1}$
  do
    Calculate: $\mathbf{r}(\mathbf{u}_i^{n+1})$
    Calculate: $\mathbf{T}(\mathbf{u}_i^{n+1})$
    Find: $\mathbf{u}_{i+1}^{n+1}$
    Calculate L^2 error: $\frac{||\mathbf{u}_{i+1}^{n+1} - \mathbf{u}_i^{n+1}||_{L^2}}{||\mathbf{u}_i^{n+1}||_{L^2}}$
    Update: $i = i + 1$
  while L^2 *error* $\geq$ *tol(NewtonRaphson)*;
  Result: $\mathbf{u}^{n+1} = \mathbf{u}_{i+1}^{n+1}$
end
Result: $\mathbf{u}^{n+1}$

Chapter 4

Numerical Tests

In the present chapter, we deal with conducting tests to check algorithmic and implementation correctness. Also suitability of the solution methodology of the code developed. Method of manufactured solutions is used for this purpose. This method involves assuming an analytical solution of a preferred form. This analytical solution satisfies the conditions (initial and boundary). The source term in CDRE is modified such that the analytical solution satisfies CDRE. Further, numerical solution of the equation is obtained using Galerkin finite element method with OSS stabilization. A comparison of numerical and analytical solutions can be made and convergence of solution error is discussed.

With the method of manufactured solutions, we test the numerical solution against the analytical one for the following cases:

1. Stationary linear CDRE
2. Stationary nonlinear CDRE
3. Transient nonlinear CDRE
4. Transient nonlinear system of coupled CDRE

Solution to the equations above are calculated for various values of the coefficients. The convective velocity is $\mathbf{a} = |\mathbf{a}|\begin{pmatrix} cos(\frac{\pi}{3}) \\ \sin(\frac{\pi}{3}) \end{pmatrix}$, where $|\mathbf{a}|$ is a norm of the velocity. The direction of the velocity field was chosen so that it did not align with the mesh. The tests performed on each of the equations are shown in Table

ID	k	$\lvert\mathbf{a}\rvert$	s	Pe	Da
Test1	10^{-4}	10^{-4}	10^{-4}	10^{-2}	4×10^{-4}
Test2	10^{-4}	10^{-4}	10	10^{-2}	40
Test3	10^{-4}	1	10^{-4}	100	4×10^{-4}
Test4	10^{-4}	1	10	100	40

Table 4.1: Tests of different coefficient values

4.1. Corresponding numerical Peclet number and numerical Damköler number are indicated.

The tests are carried on a unit square domain with zero Dirichlet condition on all boundaries. Mesh consisting of linear quadrilateral elements are used throughout the testing. The element size $h = 0.02$. The non-dimensional numbers are based on the uniform mesh in the domain and not local reduction in mesh size due to refinement carried out in regions of sharp layers. Such local refinements are carried out only to mitigate the presence of oscillatory solution in the region of sharp gradients only.

4.1 Stationary linear CDRE

Stationary linear CDRE is of the form shown in Eqn 4.1. We have spacial derivatives only. The term linear means that the coefficients k, $\mathbf{a}$ and s are not functions of the unknown u. The problem to be solved is:

$$-k\Delta u + \mathbf{a} \cdot \nabla u + su = f \quad \text{in } \Omega = [0,1] \times [0,1] \tag{4.1}$$

$$u = 0 \quad \text{on } \partial\Omega \tag{4.2}$$

Numerical solution with OSS stabilization obtained are shown in fig 4.1 for different test cases mentioned in Table 4.1. The value of source term f is unity in all the tests. Large oscillations were observed for test cases Test2, Test3 and Test4 close to the boundary where steep gradients in solution exists. We employed local mesh refinement to capture the solution and the oscillations completely vanished close to the boundary in Test2 and were limited to a few layers in Test3 and Test4 cases.

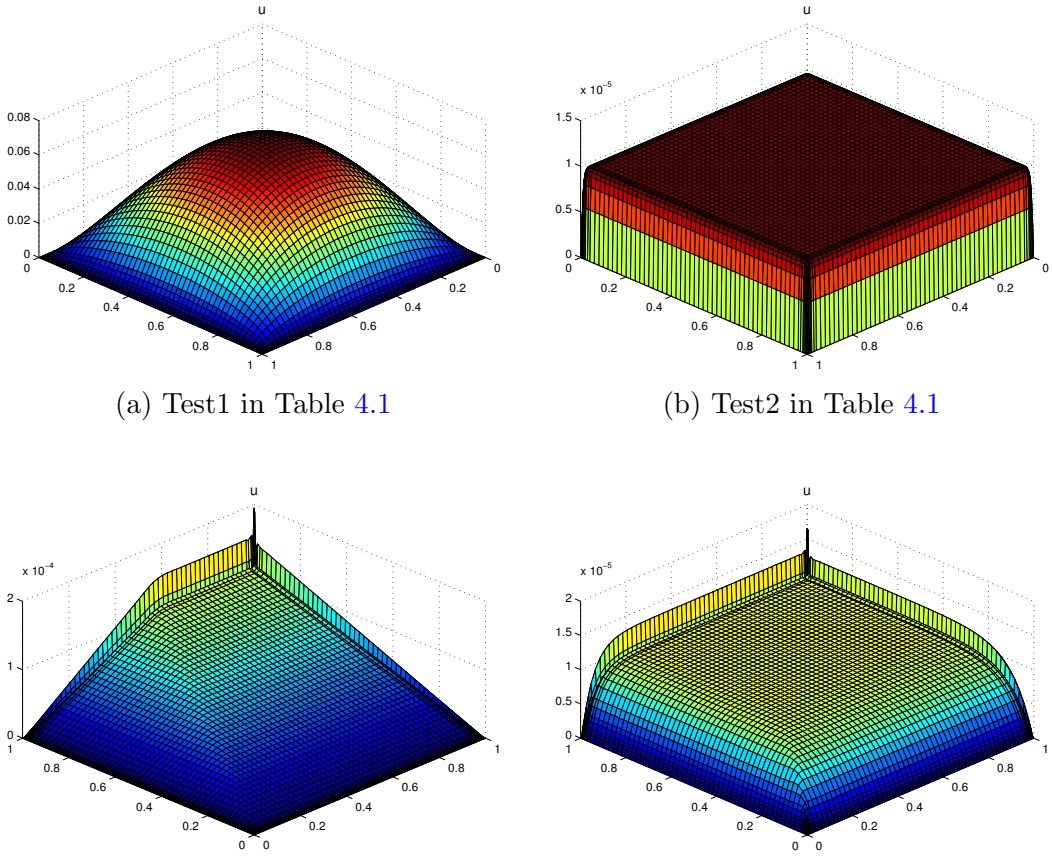

(a) Test1 in Table 4.1

(b) Test2 in Table 4.1

(c) Test3 in Table 4.1

(d) Test4 in Table 4.1

Figure 4.1: Solution plot for stationary linear CDR equation

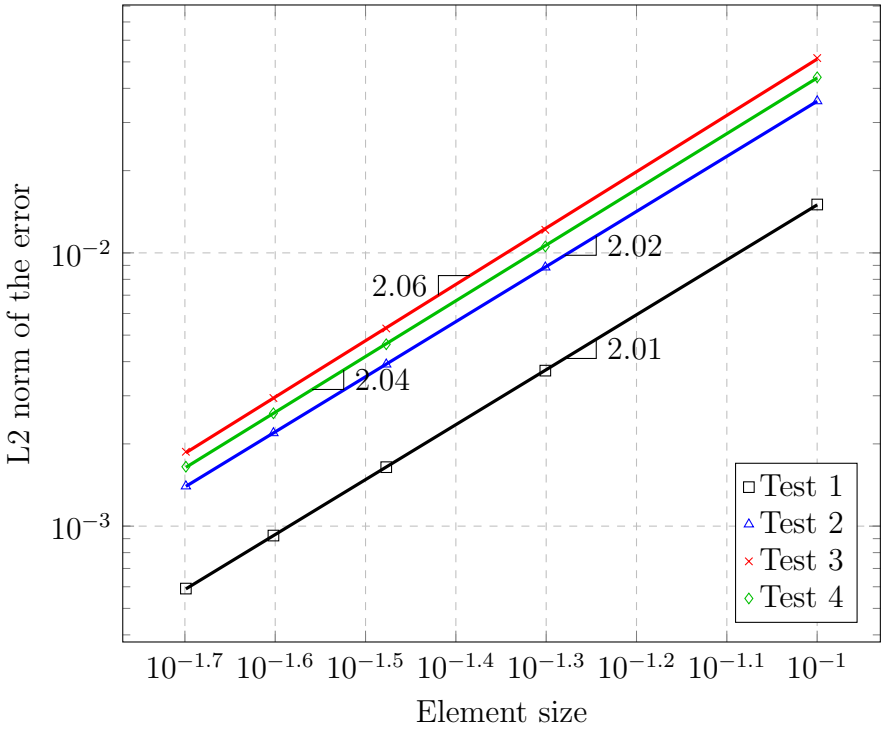

Figure 4.2: Convergence plot for stationary linear CDRE. Case 1: $u = x^2(1 - x^2)y^2(1 - y^2)$

The method of manufactured solution was now employed to study the convergence of error with decreasing size of the uniform mesh. Two cases were studies for the convergence analysis and each of the cases were subjected to the aforementioned tests. The analytical solution for each case tested for are given below and they automatically satisfy the boundary conditions. These solutions were used to build the suitable source term. They are:

$$\text{Case 1:} \quad u = \quad x^2(1 - x^2)y^2(1 - y^2) \tag{4.3}$$

$$\text{Case 2:} \quad u = \quad sin(\pi x)sin(\pi y) \tag{4.4}$$

The normalized L^2 norm of the error is a function of the mesh size. Let u_h be the piecewise linear finite element approximation of u, then the L^2 norm of the

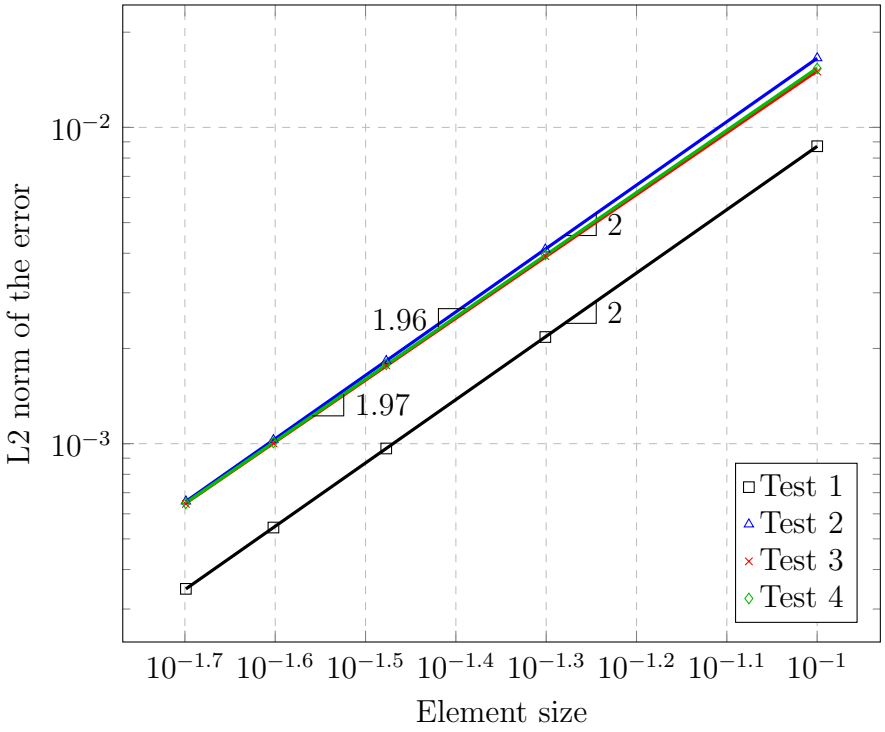

Figure 4.3: Convergence plot for stationary linear CDRE. Case 2: $u = \sin(\pi x)\sin(\pi y)$

error is given by

$$||u - u_h||_{L^2} = Ch^2||D^2u||_{L^2} \tag{4.5}$$

where C is a constant.

In our case D^2u, the second derivative of the solution, is a constant. For linear finite element approximation the L^2 error is $O(h^2)$. This means that the plot of $log(||u - u_h||_{L^2})$ vs. $log(h)$ should yield linear behaviour with slope 2

Convergence plots for Case 1 and Case 2, each for different test scenarios indicated in Table 4.1 are shown in fig 4.2 and fig 4.3 respectively. We observe that optimal convergence rates are obtained for linear finite elements with slope value of 2 for all the test cases.

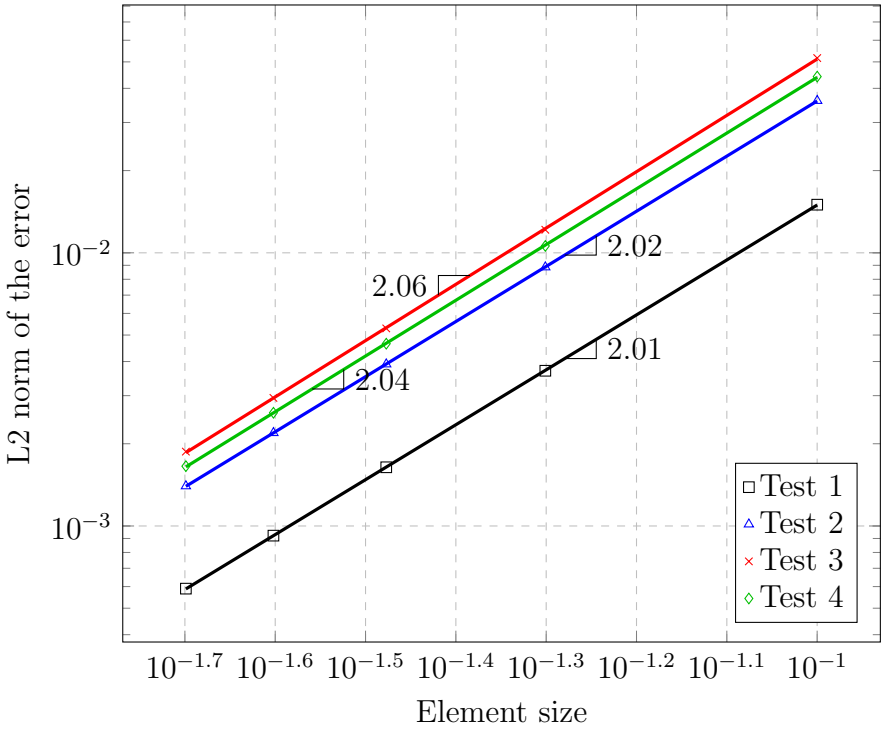

Figure 4.4: Convergence plot for stationary nonlinear CDRE. Case 1: $u = x^2(1-x^2)y^2(1-y^2)$

4.2 Stationary nonlinear CDRE

We now allow for nonlinearity in the stationary CDRE. The nonlinearity is of the of the logistic equation kind, thus the resulting CDRE is the Fisher-KPP equation. It is as shown below:

$$-k\Delta u + \mathbf{a}\cdot\nabla u - su(1-u) = f \quad \text{in } \Omega = [0,1]\times[0,1] \tag{4.6}$$

$$u = 0 \quad \text{on } \partial\Omega \tag{4.7}$$

As previously discussed, we employ method of manufactured solutions for convergence study. Two cases were tested for convergence whose analytical solutions

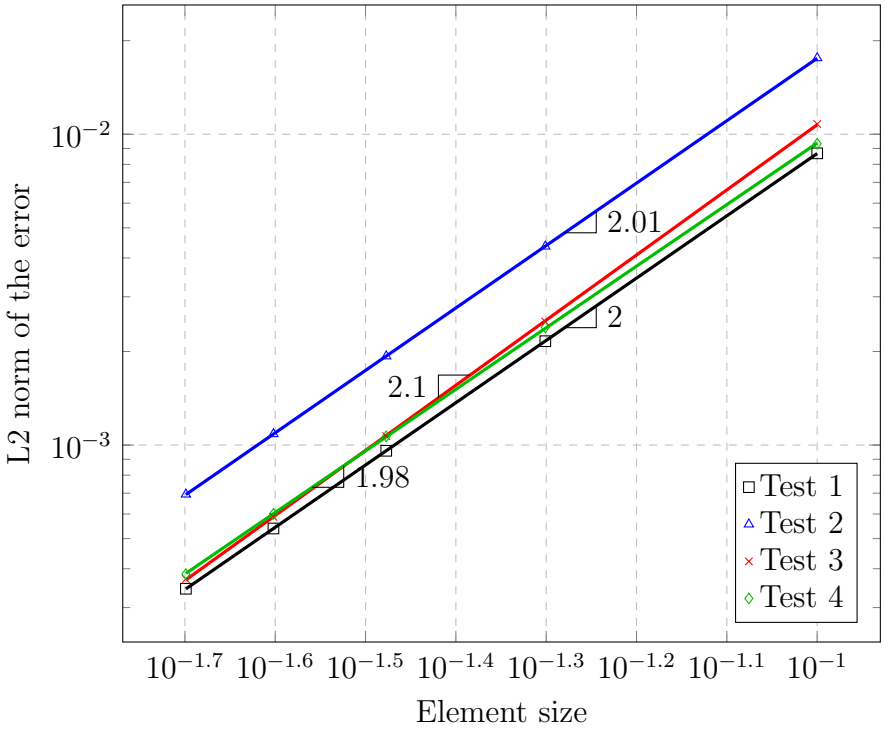

Figure 4.5: Convergence plot for stationary nonlinear CDRE. Case 2: $u = x(1-x)y(1-y)$

are given below:

$$\text{Case 1:} \quad u = \quad x^2(1-x^2)y^2(1-y^2) \tag{4.8}$$

$$\text{Case 2:} \quad u = \quad x(1-x)y(1-y) \tag{4.9}$$

The stabilization parameter (Eqn. 2.11) in this case was chosen as follows to retain dimensional homogeneity:

$$\tau^{-1} = \quad \frac{4k}{h^2} + \frac{2|\mathbf{a}|}{h} + s(1 - \max(u_i)) \tag{4.10}$$

where u_i is the solution from the previous Newton Raphson iteration.

Fig 4.4 and fig 4.5 represent the convergence plots of the Case 1 and Case 2 respectively for various test cases shown in Table 4.1. It shows optimal convergence rate with slope 2 for linear finite elements.

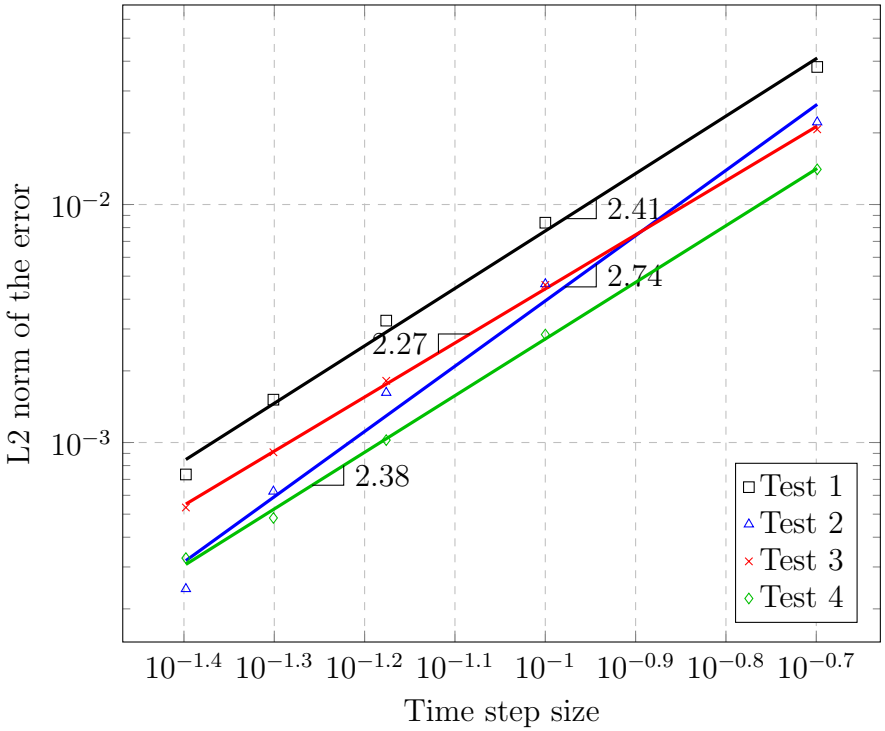

Figure 4.6: Convergence plot for transient nonlinear CDRE. Case 1: $u = 2t^3x(1-x)y(1-y)$

4.3 Transient nonlinear CDRE

We advance to transient equations in this section. Nonlinearity in reaction term of a transient CDRE is considered. The problem statement along with initial and boundary conditions are given in Eqn 4.11:

$$\partial_t u - k\Delta u + \mathbf{a}\cdot\nabla u - su(1-u) = f \quad \text{in } \Omega = [0,1]\times[0,1], t > 0 \tag{4.11}$$

$$u(t=0) = 0 \quad \text{in } \Omega \tag{4.12}$$

$$u = 0 \quad \text{on } \partial\Omega, t > 0 \tag{4.13}$$

The time interval under consideration is [0 1]. This interval was subdivided into equal time steps. For the convergence of error, we measured the error at the end of the time interval $t = 1$. BDF2 was employed for temporal discretization. As expected, with smaller time step size, the error measured in the L^2 norm

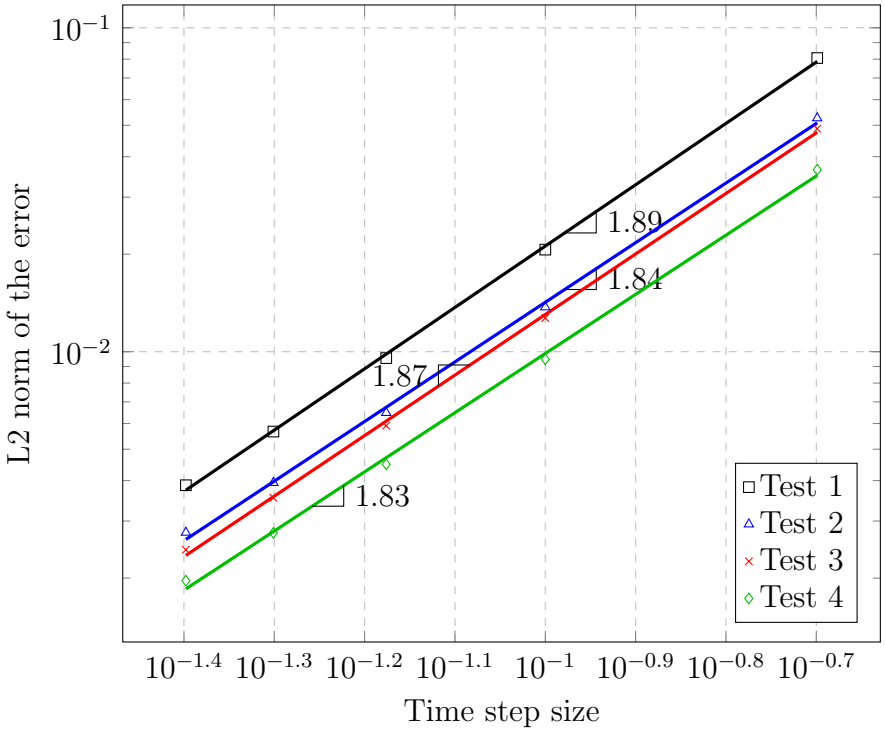

Figure 4.7: Convergence plot for transient nonlinear CDRE. Case 2: $u = \sin(\frac{\pi t}{2})x(1-x)y(1-y)$

decreased. For characteristic mesh size h and time step size δt, the behaviour of L^2 norm is given below

$$\sqrt{\sum^{n} \delta t ||u - u_h||^2_{L^2}} = \Big(C_1 h^2 + C_2(\delta t)^2\Big)||D^2 u + D_t^2 u||_{L^2} \tag{4.14}$$

C_1 and C_2 are constants, D^2 and D_t^2 are spacial and temporal second derivatives. Since we are interested in the convergence of solution with time, we consider a fine mesh so that the error contribution due to spacial discretization is minimum. Hence, the dependency of error on time is $O(\delta t^2)$. The convergence plot of normalized error measured in L^2 norm, we anticipate a slope of 2.

Two cases with different time dependencies are considered and the correspond-

ing analytical solutions are listed below:

$$\text{Case 1:} \quad u = \quad 2t^3 x(1-x)y(1-y) \tag{4.15}$$

$$\text{Case 2:} \quad u = \quad \sin(\frac{\pi t}{2})x(1-x)y(1-y) \tag{4.16}$$

The stabilization parameter τ was considered constant for a given time step and was calculated using the solution at the previous time step u^n. It was not updated for every Newton Raphson iteration as carried out for the stationary nonlinear case. The choice was made in order to reduce computational expenses. The drawback is that the rate of convergence is linear and not quadratic. This is demonstrated in the predator-prey example presented later in this document. The stabilization parameter is

$$\tau^{-1} = \quad \frac{4k}{h^2} + \frac{2|\mathbf{a}|}{h} + s(1 - \max(u^n)) \tag{4.17}$$

Solution errors in the L^2 norm for different time steps sizes were calculated for various test cases in Table 4.1 and are plotted in Fig 4.6 and Fig 4.7 respectively. In Case1, we obtain optimal convergence rates and in Case2, the slope is less than 2. Case 2 offers a small flattening of the error slope with decrease in time step size. The reason for the behaviour may be due to spacial error becoming significant in affecting the slope for the convergence in time. This can be mitigated with further finer meshes.

4.4 Transient nonlinear system of coupled CDREs

A system of coupled transient CDREs is considered in the present section. The coupling is in the nonlinear reaction term only. The solution unknowns are denoted by u_1 and u_2. The nonlinearity in reaction is of the Fisher-KPP form for both equations. The problem statement is presented in Eqn 4.18

Find u_1 and u_2 such that

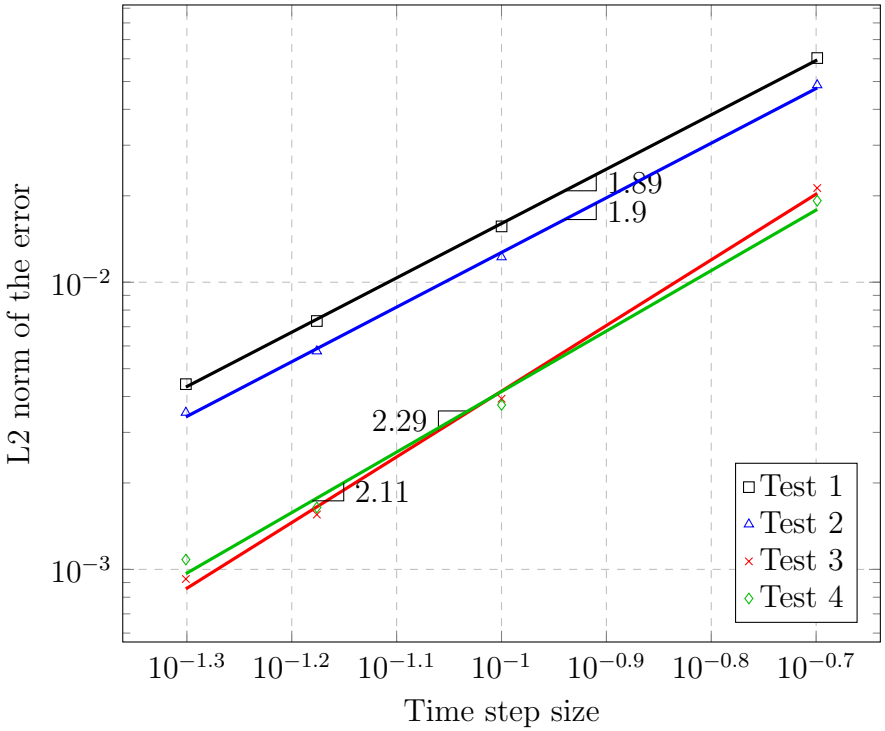

Figure 4.8: Convergence plot for transient nonlinear system of CDREs. $u_1 = t^2x(1-x)y(1-y)$

$$\begin{bmatrix}\partial_t u_1\\ \partial_t u_2\end{bmatrix} - \begin{bmatrix}k_1\Delta u_1\\ k_2\Delta u_2\end{bmatrix} + \begin{bmatrix}\mathbf{a}_1\cdot\nabla u_1\\ \mathbf{a}_2\cdot\nabla u_2\end{bmatrix} - \begin{bmatrix}s_{11} & s_{12}\\ s_{21} & s_{22}\end{bmatrix}\begin{bmatrix}u_1(1-u_1)\\ u_2(1-u_2)\end{bmatrix} = \begin{bmatrix}f_1\\ f_2\end{bmatrix} \quad \text{in } \Omega = [0,1]\times[0,1] \tag{4.18}$$

$$u_1(x,y,t=0) = \quad u_2(x,y,t=0) = 0 \qquad \text{in } \Omega \tag{4.19}$$

$$u_1(x,y,t>0) = \quad u_2(x,y,t>0) = 0 \qquad \text{on } \partial\Omega \tag{4.20}$$

In the Newton Raphson linerization loop, iterations were performed until the respective differences between successive solutions of both u_1 and u_2 were below the specified tolerance.

Again, method of manufactured solutions was used to perform the convergence study. The case considered with the analytical solution is shown below. u_1 and u_2 behave differently in time since the convergence study in time is of interest in

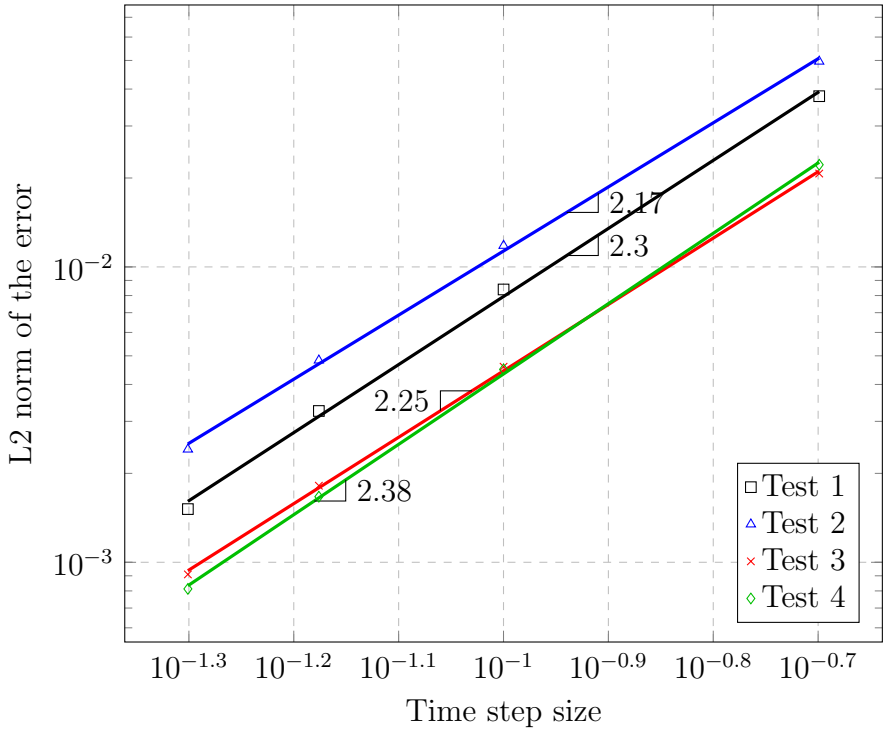

Figure 4.9: Convergence plot for transient nonlinear system of CDREs. $u_2 = \sin(\frac{\pi t}{2})x(1-x)y(1-y)$

this case. They are given by:

$$u_1 = \quad t^2 x(1-x)y(1-y) \tag{4.21}$$

$$u_2 = \quad \sin(\frac{\pi t}{2})x(1-x)y(1-y) \tag{4.22}$$

Fig 4.8 and fig 4.9 show the convergence in time for u_1 and u_2 respectively. Optimal convergence is obtained with slope 2. Hence we are assured of a bug-free, correct implementation of the finite element code with OSS stabilization, Newton Raphson linearization and BDF2 time stepping.

In the next section, we apply the code for various examples to demonstrate the effectiveness of the developed code in terms of capturing of sharp layers, flexibility of implementation and effectiveness of handling large Pe and Da numbers.

Chapter 5

Numerical Examples

We present the application of finite element code with OSS stabilization in various scenarios where CDRE needs to be solved for. Examples of CDRE in flow through a channel and cavity flow are highlighted. These cases demonstrate the ability of stabilization in obtaining an oscillation-free solution for a transient nonlinear CDRE. Also a predator-prey model consisting of a transient nonlinear system of coupled CDREs is solved.

We would like to convey a strong message that the present formulation is capable of solving a number of applications of CDRE with nonlinear reaction. We would like to highlight the stability of the method even for high Pe and Da numbers that are traditionally not solvable by Galerkin finite element method. Also the formulation is able to capture sharp layers in the solution with selective mesh refinement. The error remains bounded and the method offers optimal convergence

5.1 Channel flow

Pressure driven, fully-developed laminar fluid flow through a channel is a well studied problem. A characteristic parabolic velocity profile is developed across the cross-section of the channel. A no-slip boundary imposes zero velocity along the walls. The fluid achieves maximum velocity along the center. Examples of such scenario include Couette flow (laminar viscous flow between two parallel

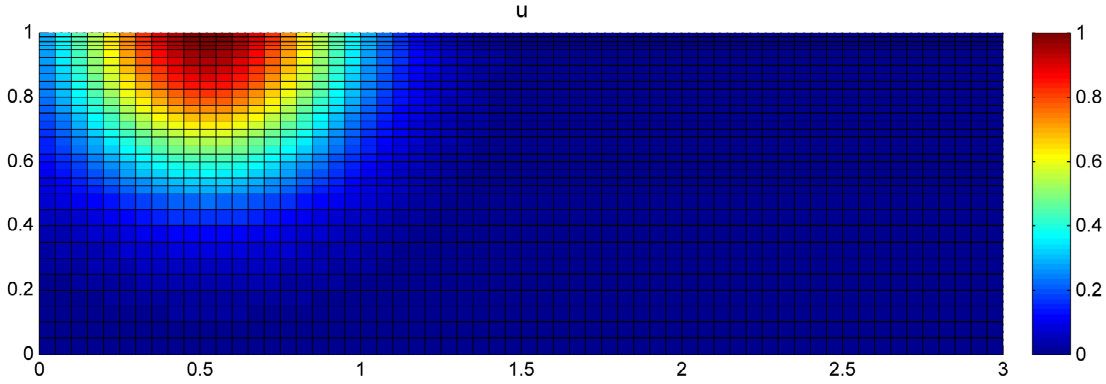

Figure 5.1: Channel flow: Initial solution for test cases

plates), Hagen-Poiseuille flow (laminar flow in a closed conduit), etc.

In the present example we study the spacio-temporal evolution of a quantity of interest u governed by a nonlinear CDRE when subjected to the convective velocity field of a channel flow. In particular we chose Fisher-KPP equation. These model population growth of bacteria and hence the solution can be considered as the time evolution of a bacteria colony in a pipe flow.

The domain of the problem is a rectangle of dimension $[0\ 3] \times [0\ 1]$. The left and right boundaries are inlet and outlet respectively. The top and bottom boundaries represent rigid walls with no-slip velocity. The parabolic velocity profile shown in fig 5.2 is unaltered by the concentration of the species. Hence there is a one-way coupling between the flow problem and the CDRE. The initial condition for the problem consists of a normal distribution of the species close to the wall as shown in fig 5.1. The problem is stated as follows

$$\text{Find } u \text{ such that}$$

$$\partial_t u - k\Delta u + \mathbf{a}\cdot\nabla u + su(1-u) = f \quad \text{in } \Omega = [0\ 3] \times [0\ 1] \tag{5.1}$$

$$\mathbf{a}(x,y,t) = \begin{pmatrix} 4(y-y^2) \\ 0 \end{pmatrix} \tag{5.2}$$

$$\text{Initial condition: Fig 5.1}$$

$$u(x, y=0, t) = u(x, y=1, t) = 0 \tag{5.3}$$

$$k\mathbf{n}\cdot\nabla u|_{x=0,y,t} = k\mathbf{n}\cdot\nabla u|_{x=3,y,t} = 0 \tag{5.4}$$

The maximum velocity attained at the centre is of magnitude unity. We

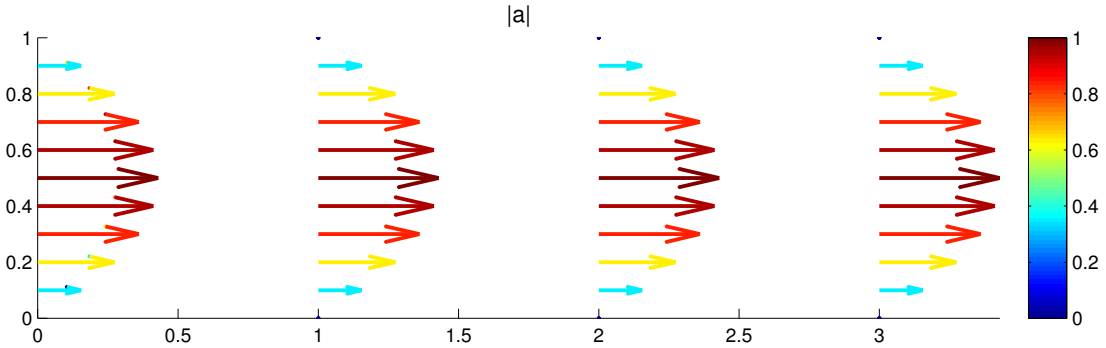

Figure 5.2: Channel flow velocity field for test cases

ID	k	s	h	Pe	Da
Case1	10^{-4}	0.1	0.025	125	0.4
Case2	10^{-4}	1	0.02	100	4
Case3	10^{-4}	5	0.02	100	20

Table 5.1: Channel flow test cases for different coefficient values

perform the tests as shown in Table 5.1. We would like to highlight that the Pe number is very high at 100 to 125. Moreover, each case corresponds to various strengths of reaction coefficient and thereby different Da number.

The result for different time steps for Case1, Case2 and Case3 are shown in figs 5.3, 5.4 and 5.5 respectively. We can observe that in fig 5.3 with small value of reaction coefficient s, we can obtain a smooth solution with a relatively coarser mesh. Since advection is dominant to reaction, generation or destruction is not dominant. For the case when $s = 1$ shown in fig 5.4, we observed that a finer mesh was required to capture the solution. If a coarser mesh was used, the error built-up from each consecutive time step resulted in non-convergence of the solution at a later time step. This is one the drawbacks of using Newton Raphson for linearization. This can be overcome to a certain extent by introducing relaxation or using other linearization techniques. This is not carried out as it is not in the scope of this study. For the case with $s = 5$ and Da $= 20$, the reaction term has a dominant effect in the proliferation of the species. The solution is oscillation free and sharp layers are captured well. Hence we have demonstrated that finite element method with OSS stabilization can successfully solve problems

with moderately large convection and reaction terms. Newton Raphson iteration was unable to resolve splitting into 'plumes' in the case with $s = 5$ when large advection field cuts through a dense concentration of species generated by large reaction. This is one of the limitations of our preferred linearization technique.

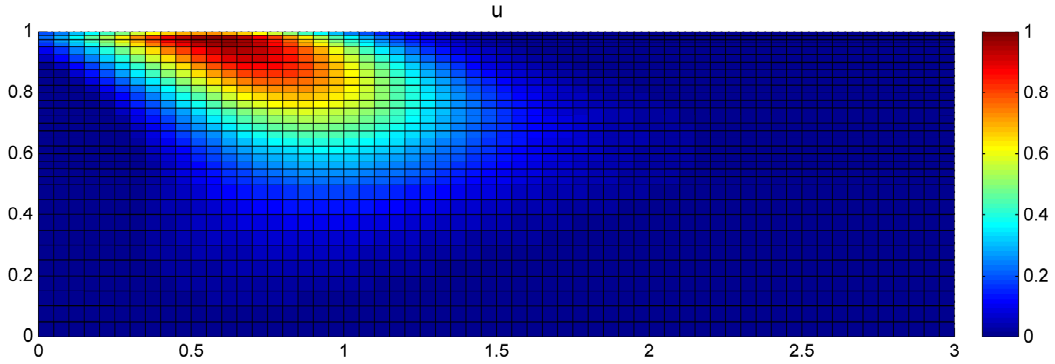

(a) $t = 0.5$

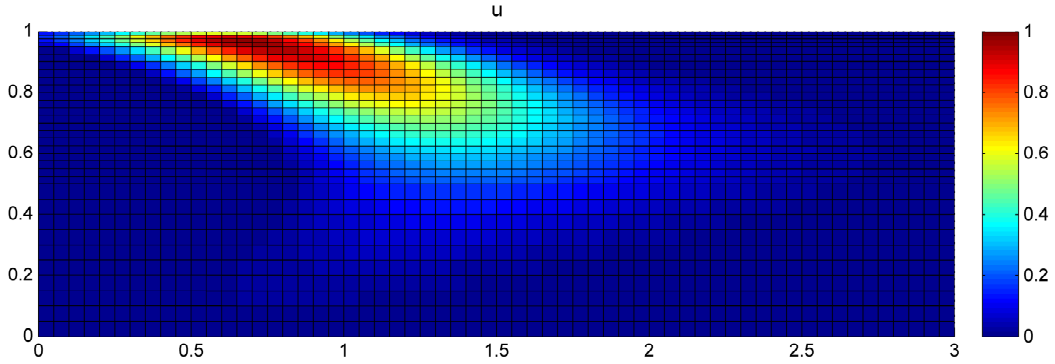

(b) $t = 1.0$

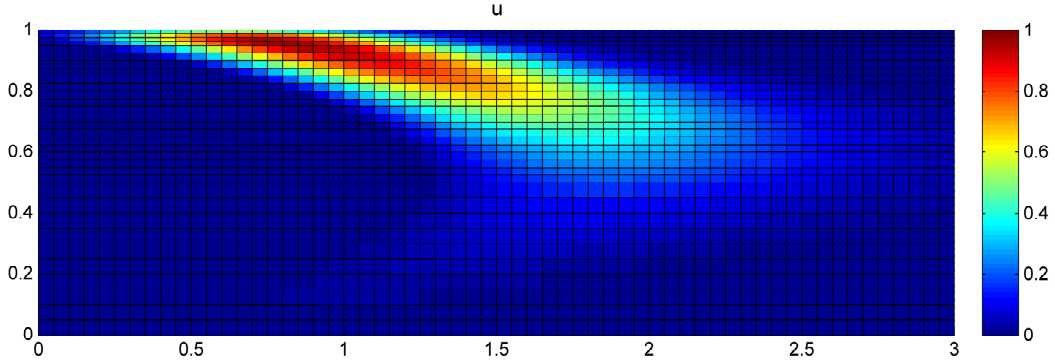

(c) $t = 1.5$

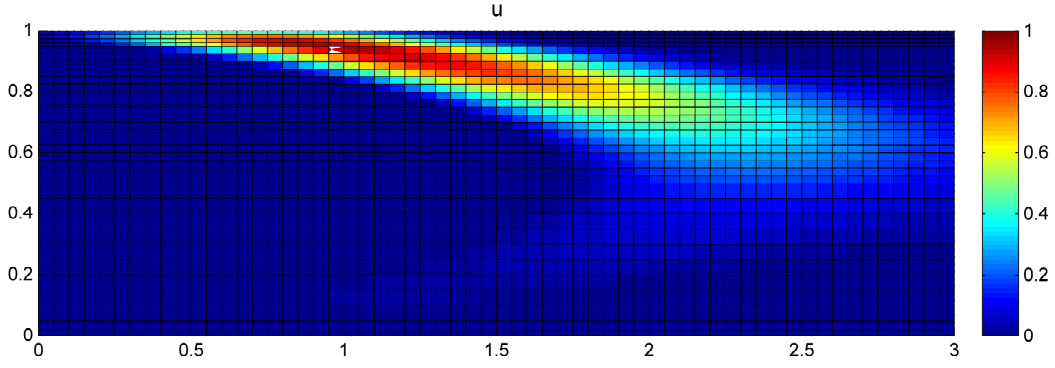

(d) $t = 2.0$

Figure 5.3: Channel flow for $s = 0.1$ with $\mathrm{Pe} = 125$ and $\mathrm{Da} = 0.4$

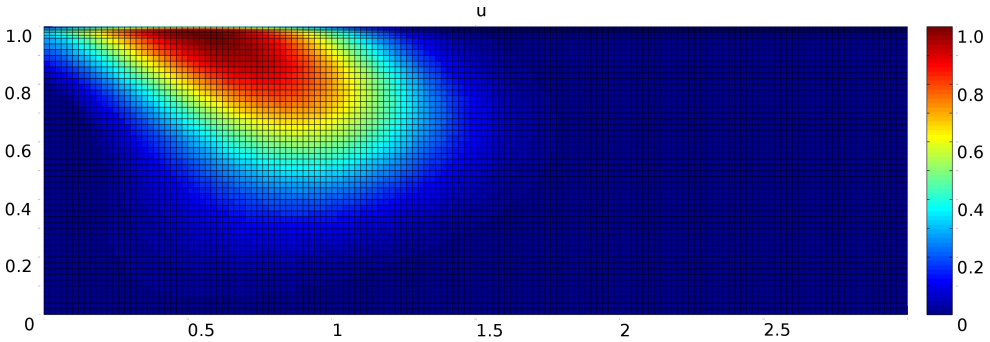

(a) $t = 0.4$

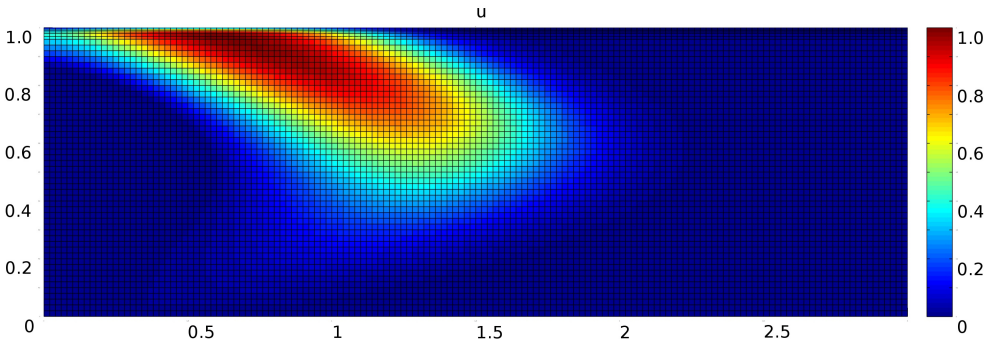

(b) $t = 0.8$

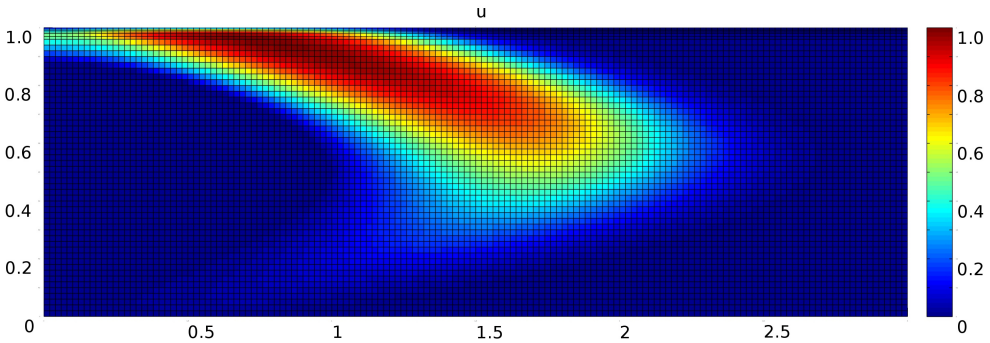

(c) $t = 1.2$

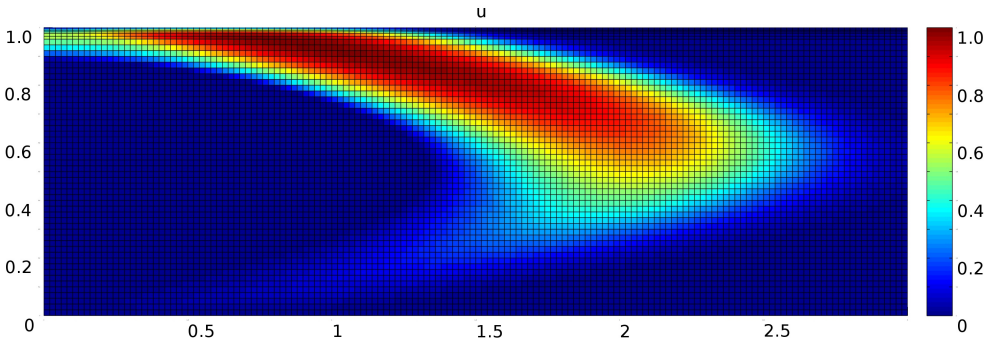

(d) $t = 1.6$

Figure 5.4: Channel flow for $s = 1$ with Pe $= 100$ and Da $= 4$

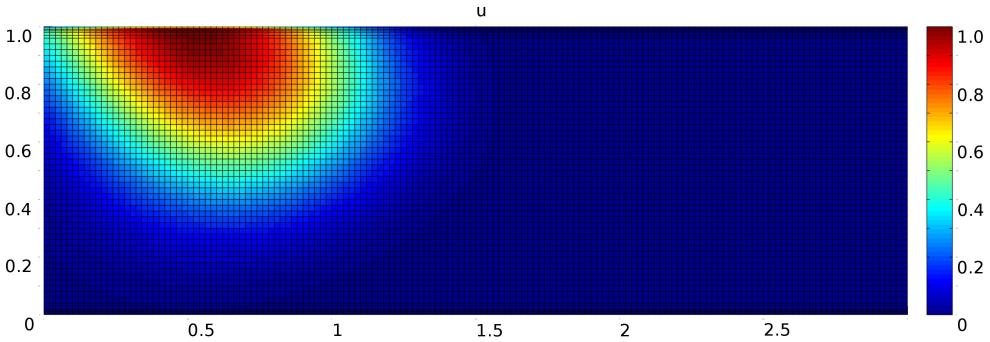

(a) $t = 0.14$

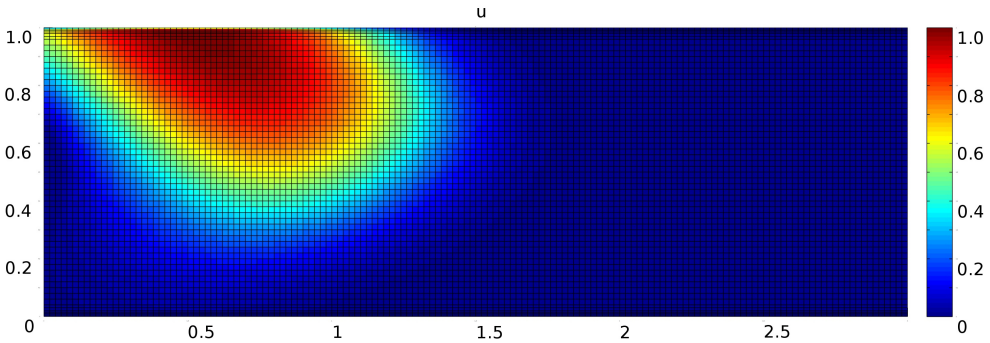

(b) $t = 0.28$

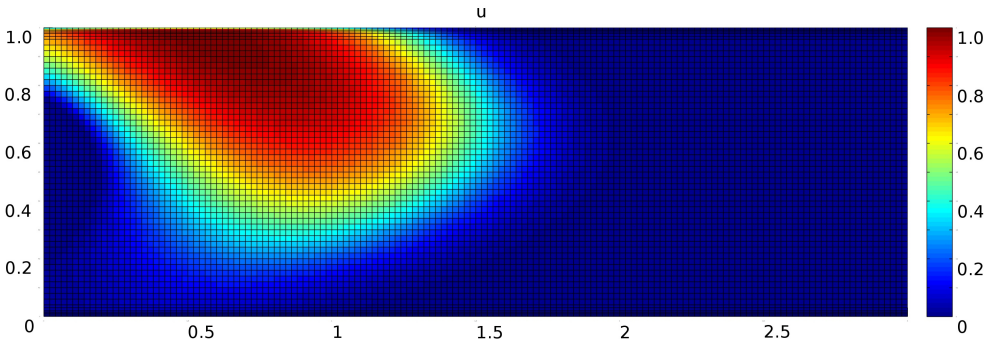

(c) $t = 0.42$

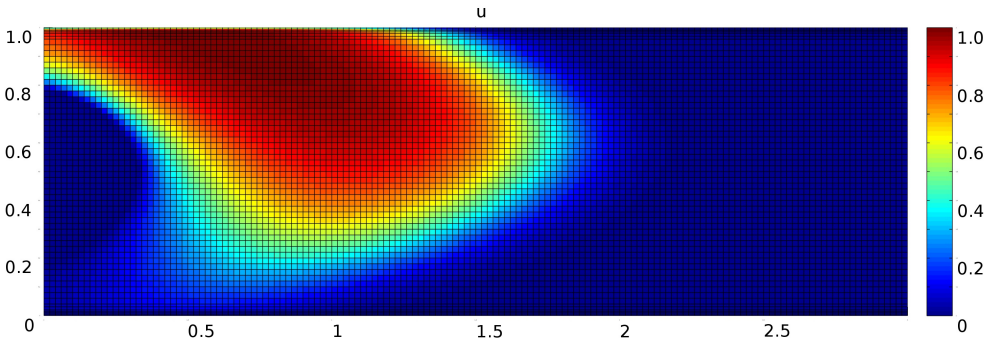

(d) $t = 0.56$

Figure 5.5: Channel flow for $s = 5$ with $\mathrm{Pe} = 100$ and $\mathrm{Da} = 20$

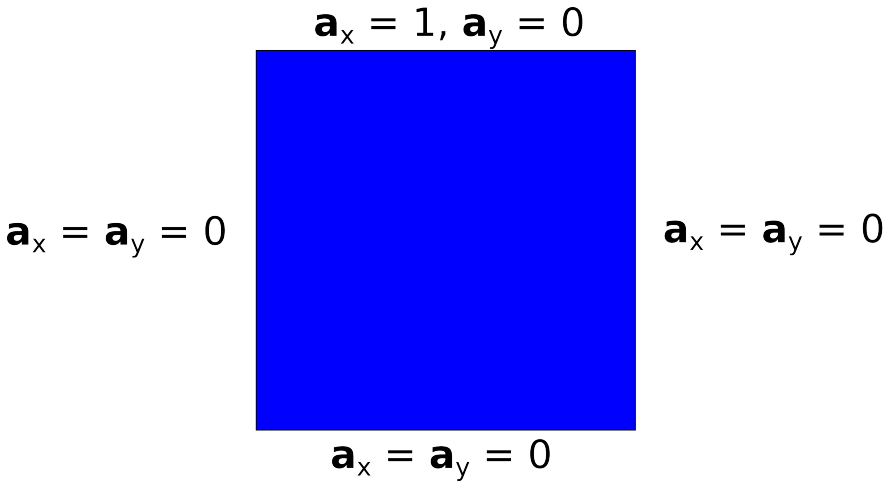

Figure 5.6: Cavity flow domain and boundary conditions

5.2 Cavity flow

A lid-driven cavity flow is a popular benchmark problem in CFD. It is a flow problem in a rectangular domain with three stationary walls and one moving boundary (usually the top). Incompressible Navier-Stokes equation in its non-dimensional form is solved. The domain and the boundary conditions for the flow problem employed in the study are shown in fig 5.6. The velocity field generated is dependent on the Reynold's number (Re). It is observed that a steady field is obtained upto Re = 10000, after which the solution is transient. Hence, we restrict ourselves to below this Re limit. Steady state velocity fields for Re = 200 and 4000 shown in fig 5.7 are used for our tests since they represent distinct features in their vortical structures.

Transient, nonlinear CDRE equation of Fisher-KPP kind is solved in the domain with the advection field of the cavity flow problem. Cavity flow generates a central large eddy and smaller eddies along the corners depending on the Re. Such velocity fields provide challenges in obtaining numerical solution to the CDRE. The aim of this section is to demonstrate the capability of OSS stabilized finite element solution in providing smooth solutions to CDRE with high Pe and Da numbers in a complex flow field. An initial distribution of the quantity of interest (species) used as the initial condition is shown in fig 5.8. The evolution of the distribution is the solution sought after. In the present case, diffusion is

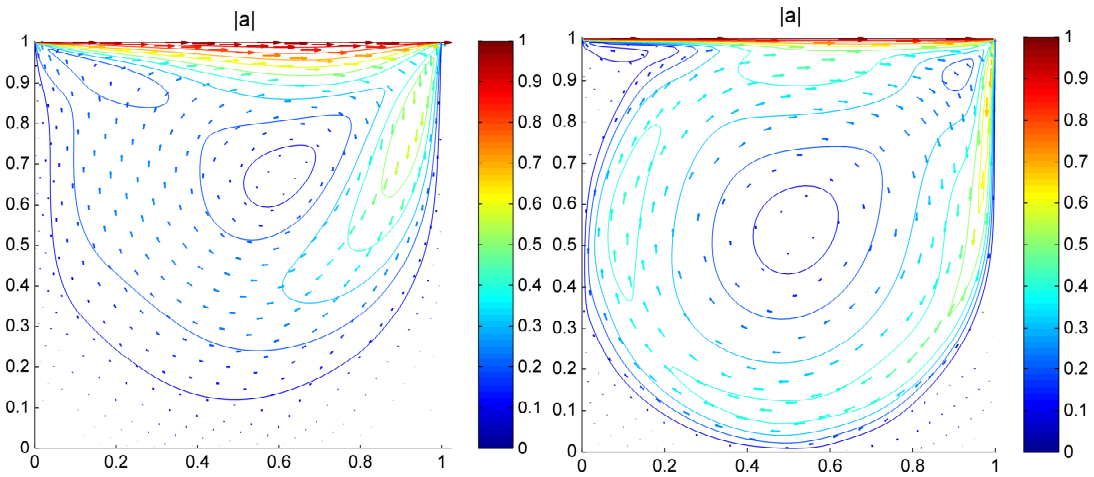

(a) $Re = 200$ (b) $Re = 4000$

Figure 5.7: Cavity flow velocity field for test cases

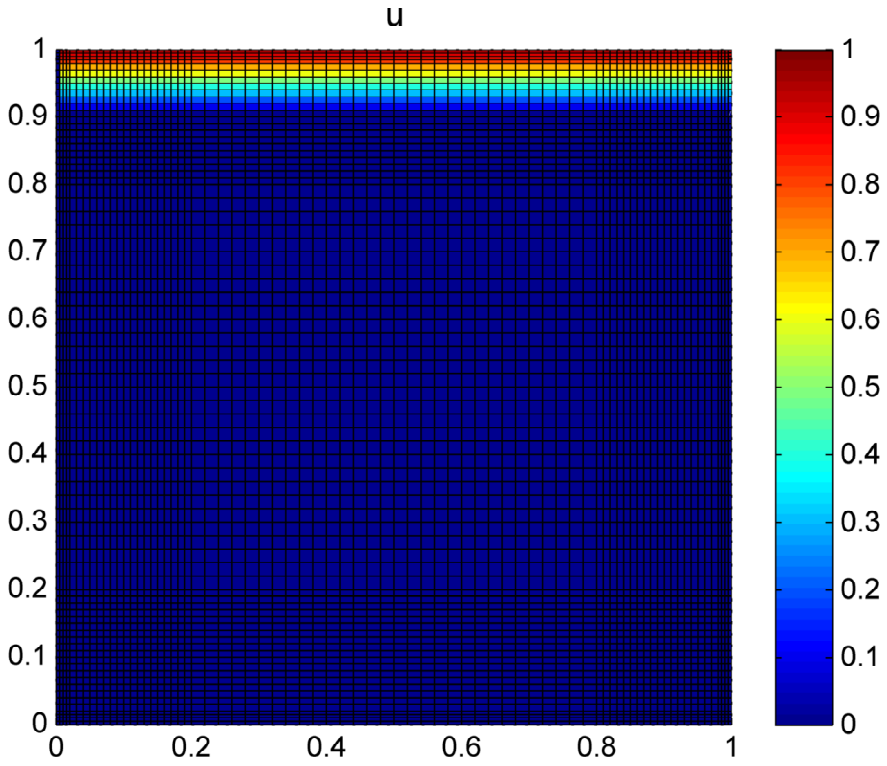

Figure 5.8: Cavity flow: Initial solution for test cases

weak with value $k = 10^{-4}$ and reaction is strong with $s = 1$. The maximum velocity on the top surface has unit magnitude as shown in fig 5.7. The CDRE problem is stated as follows

$$\text{Find } u \text{ such that}$$

$$\partial_t u - k\Delta u + \mathbf{a} \cdot \nabla u + su(1-u) = f \quad \text{in } \Omega = [0\ 3] \times [0\ 1] \tag{5.5}$$

$$u(x = 0, y, t) = u(x = 1, y, t) = u(x, y = 0, t) = 0 \tag{5.6}$$

$$\mathbf{a} \text{ is the velocity field shown in Fig 5.7}$$

$$\text{Initial condition: Fig 5.8}$$

The problem consists of large convection and reaction processes relative to diffusion. We thus expect sharp layers and hence considerations for mesh size and selective refinement is important. The problem was initially solved with a coarse mesh to determine the distribution of u. For Re = 200, u was found to get transported in the whole domain, hence an overall finer mesh ($h = 1/75$) was chosen with a thin refinement zone along the boundary. For Re = 4000, u was found to evolve being transported close to the domain boundaries. Hence an overall coarse mesh ($h = 1/50$) with thicker zone of refinement from the boundary was found to be good choice. Pe and Da numbers are determined based on the mesh size which is different for the two cases considered (for Re = 200, Pe = 67 and Da = 1.8 . and for Re = 4000, Pe = 100 and Da = 4). It is to be noted that although Da number seem close to unity in the cases above, these cases with finer meshes are employed only to capture the transition of solution through the sharp layer via multiple elements. But it is not necessary since the initial coarse mesh with higher Da was able to produce a globally smooth solution.

5.2.1 CDRE solution for Re = 200

Solution to transient nonlinear CDRE whose advection field is from the cavity flow problem with Re = 200 is shown in fig 5.9. We can observe dominant advection and reaction phenomenon driving the change. The thickness of layer due to diffusion is small, hence a finer mesh is preferred to capture the transition although it is not necessary. Also the effect of a finer mesh in increasing the resolution of the solution obtained in fig 5.9(g) clearly close to the right boundary.

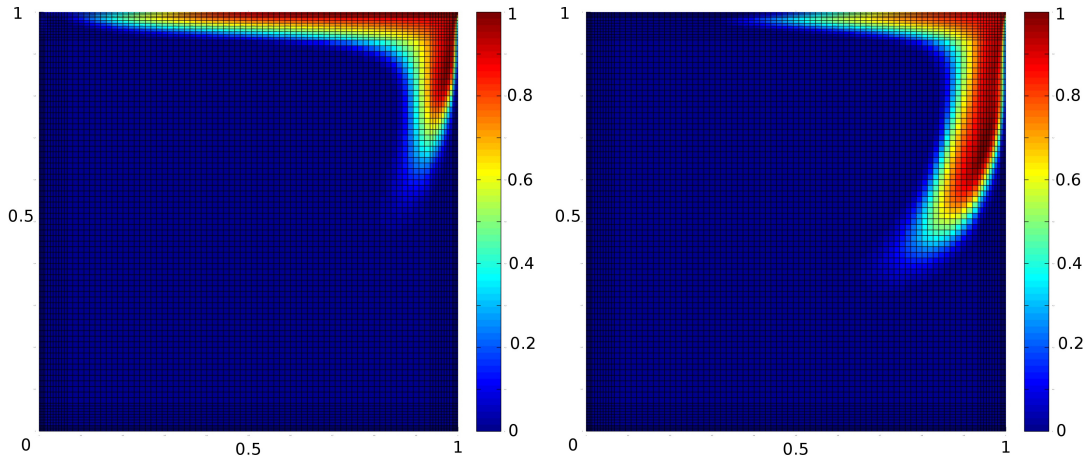

(a) $t = 0.5$ (b) $t = 1.0$

(c) $t = 1.5$ (d) $t = 2.0$

Figure 5.9: Cavity flow: CDRE solution snapshots for Re = 200, Pe = 67 and Da = 1.8

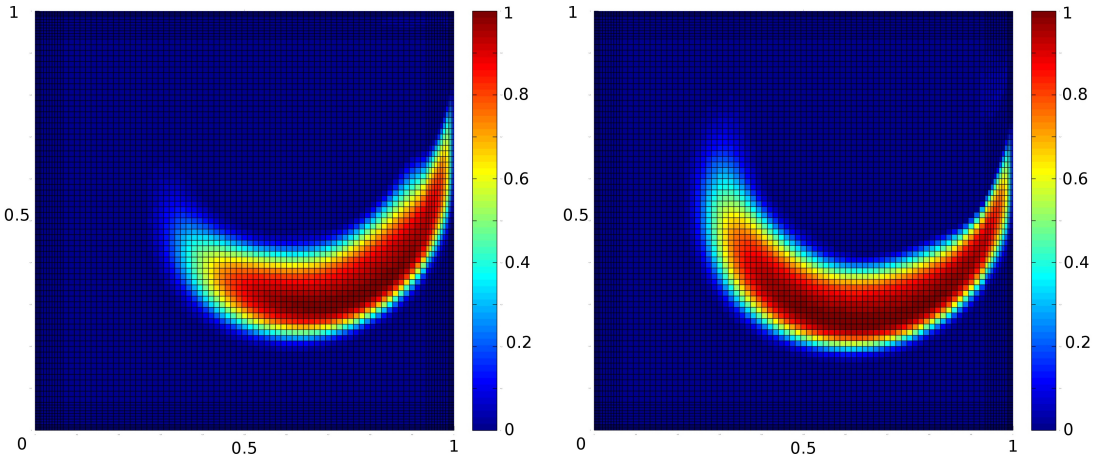

(e) $t = 2.5$ (f) $t = 3.0$

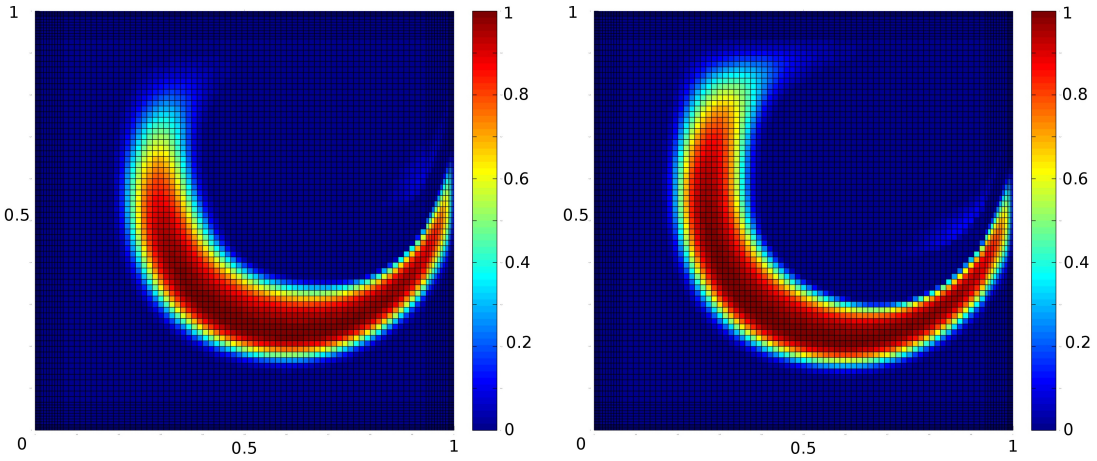

(g) $t = 3.5$ (h) $t = 4.0$

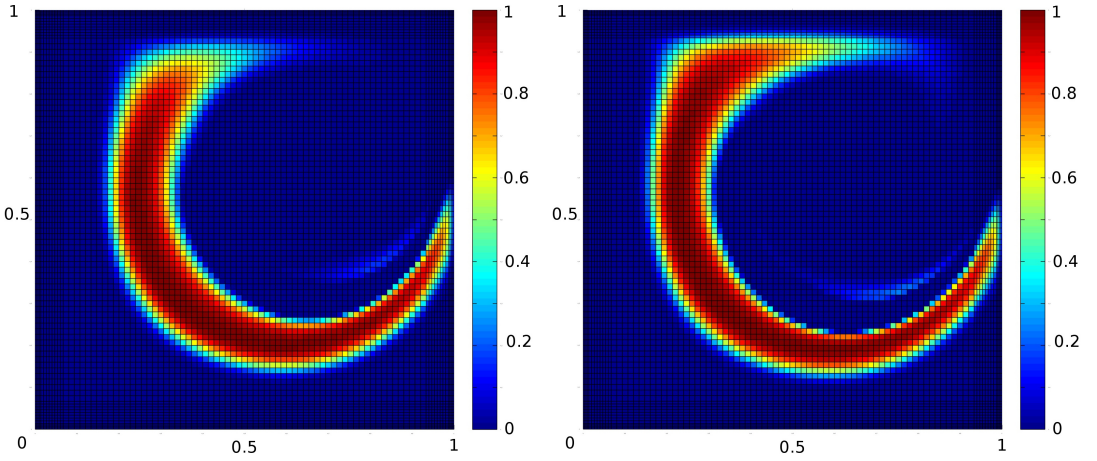

(i) $t = 4.5$ (j) $t = 5.0$

Figure 5.9: Cavity flow: CDRE solution snapshots for Re = 200, Pe = 67 and Da = 1.8

5.2.2 CDRE solution for Re = 4000

In the solution for Re = 4000 shown in fig 5.10 the first observation is that the species caught up in small eddies at this flow regime are captured well. As remarked in the previous case, the thickness of transition layer is small and a fine mesh helps if accurate monitoring of the transition zone is critical. Smooth non-oscillatory solutions are obtained.

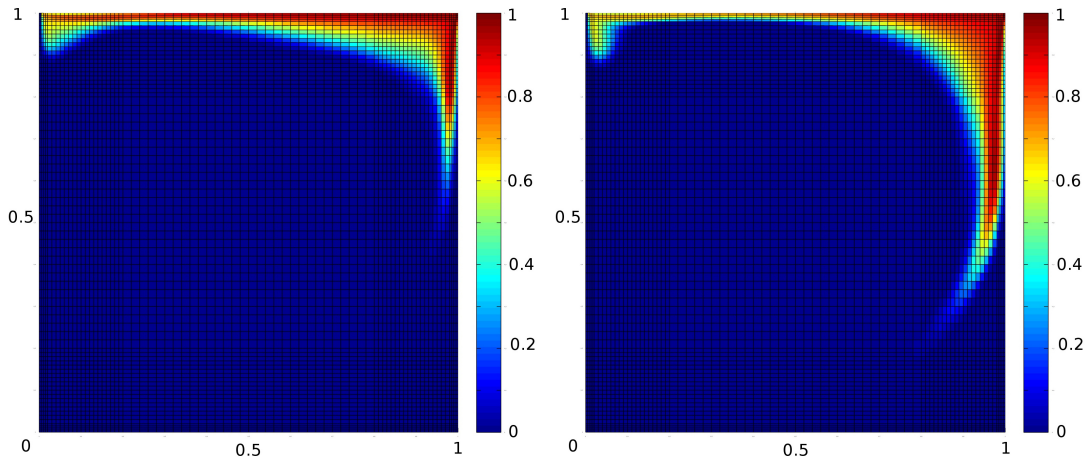

(a) $t = 0.5$ (b) $t = 1.0$

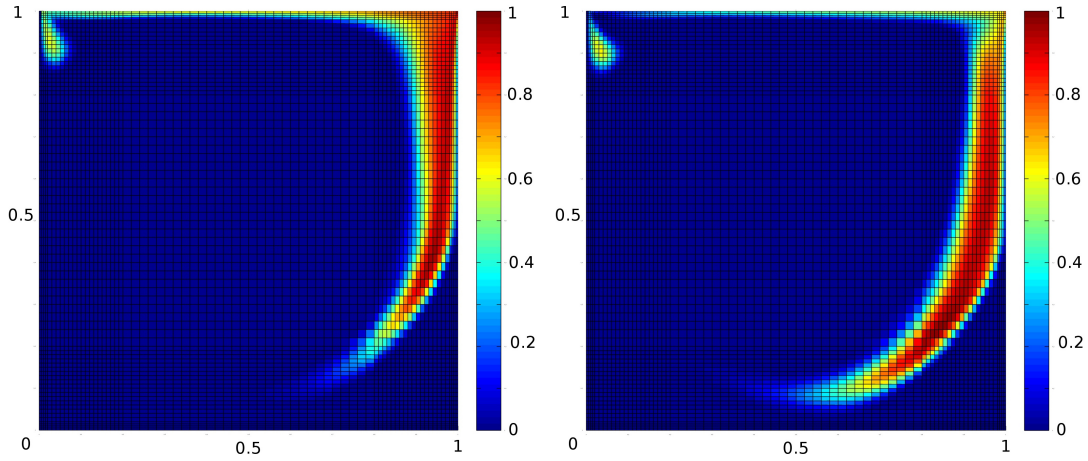

(c) $t = 1.5$ (d) $t = 2.0$

Figure 5.10: Cavity flow: CDRE solution snapshots for Re = 4000, Pe = 100 and Da = 4

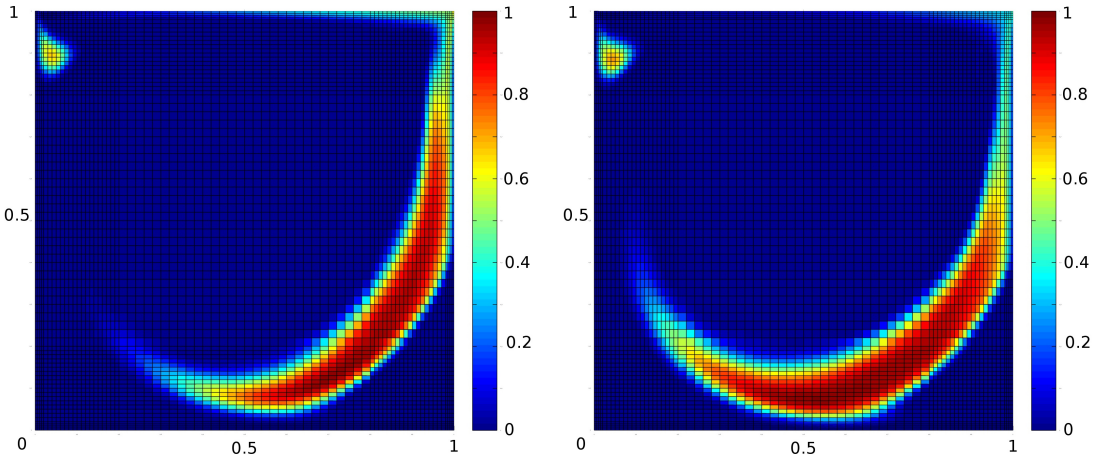

(e) $t = 2.5$ (f) $t = 3.0$

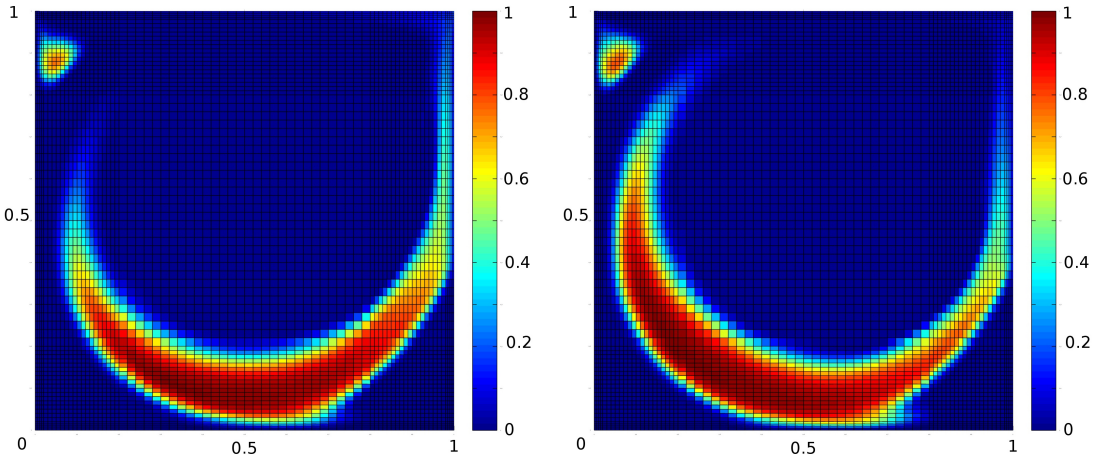

(g) $t = 3.5$ (h) $t = 4.0$

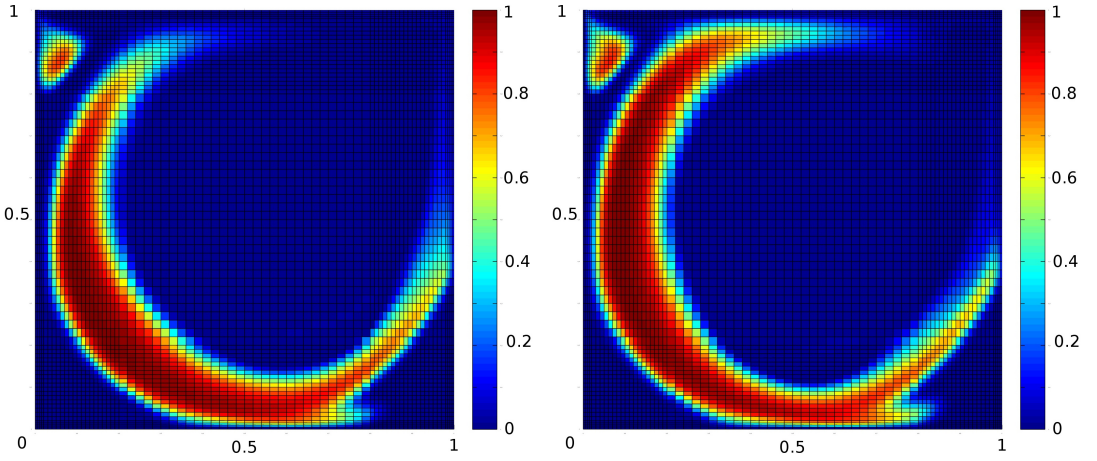

(i) $t = 4.5$ (j) $t = 5.0$

Figure 5.10: Cavity flow: CDRE solution snapshots for Re = 4000, Pe = 100 and Da = 4

5.3 Predator-prey system

As an example of coupled system of nonlinear equations, we consider the predator-prey model in ecological interactions describing population dynamics in terms of spatially and temporally continuous quantity such as density function. Also, here we consider models with time-continuous properties.

When population studies were required to be initiated, it was found that species specific studies were discouragingly complicated for a system with large number of interacting entities. The easiest simplification was to reduce the complexity to just the interaction between two 'functional groups', zooplanktons and photoplanktons. This binary description worked good in empirical sense too. The next step was to formulate the model and discover the properties such as existence, stability and bounds of the solution, periodicity or pattern formation and bifurcation. It is not the intention of the present study to delve in these mathematical aspects. Rather, when such system is required to be solved for different values of parameters of the equations, challenges in obtaining numerical solution are encountered when the scales of these parameters are hugely different. To address and tackle these challenges is the main intention.

In the next section, we briefly describe the origin of the predator-prey model used in the present work. Much of the details about the model can be obtained in the reference book by Malchow et al.Malchow [2008].

5.3.1 Formulation of predator-prey model

A generalized starting point for a closed system predator-prey modelling is the transient diffusion reaction equation as mentioned in the first chapter. This is of a general form shown in Eqn 5.7

$$\begin{aligned} \partial_t u_1 = &\quad k_1 \Delta u_1 + P(u_1) - E(u_1, u_2) \\ \partial_t u_2 = &\quad k_2 \Delta u_2 + \kappa E(u_1, u_2) - \mu(u_2) \end{aligned} \tag{5.7}$$

In Eqn 5.7, u_1 and u_2 represent the population densities of the prey and predator respectively. $P(u_1)$ is the prey population growth function. $E(u_1, u_2)$ represents the act of predation, resulting in a decline of prey and growth of preda-

tor populations. κ is the predation efficiency which determines the effectiveness of predation on the growth of predator population. $\mu(u_2)$ quantifies predator mortality.

Hence the prey equation consists of diffusion or spreading of prey population, its growth by reproduction P and its demise by predation E. On the other hand, predator equation consists of its spreading, its growth by predation E (with κ efficiency, where $0 \leq \kappa \leq 1$) and its death by mortality μ.

One of the popular approaches to model the functions P, E and μ is shown in Eqn 5.8 and 5.9

$$\partial_t u_1 = k_1 \Delta u_1 + C u_1 (1 - \frac{u_1}{K}) - B \frac{u_1 u_2}{u_1 + H} \tag{5.8}$$

$$\partial_t u_2 = k_2 \Delta u_2 + \kappa B \frac{u_1 u_2}{u_1 + H} - M u_2 \tag{5.9}$$

Here, predator functional response to prey density E, is modelled by the often-used so-called Hollinger type II. B represents the predation rate and the parameter H has the meaning of the half-saturation prey density. For prey population growth model, logistic equation is used. C represents the prey growth rate and K is the carrying capacity of the system, which denotes the maximum population of prey supported by the domain. Also, the predator mortality μ is given by a linear term.

Adding to this, a seasonal migration pattern or migrations towards regions of resource availability can be introduced via the convection term. This models the bulk movement of populations and is the origin of $\mathbf{a}_1$ and $\mathbf{a}_2$. We combine all of the above processes and represent it in terms of our notation. We assume the carrying capacity K to be unity. Resulting predator-prey model is shown in Eqn 5.10 with suitable initial and boundary conditions. Here coupling of equations in the reaction terms can be observed and hence our code for transient coupled

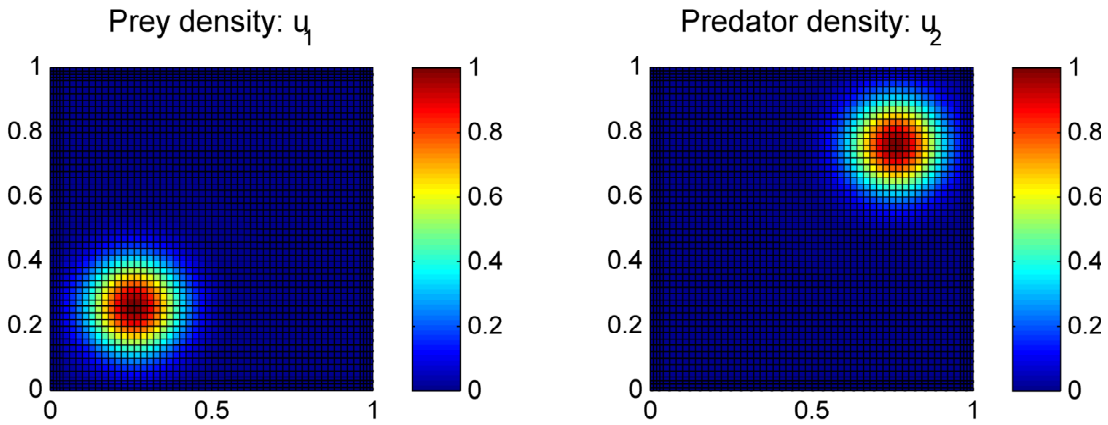

Figure 5.11: Predator-prey initial solution for test cases

ID	s_{11}	s_{12}	s_{21}	s_{22}
Case1	0	0	0	0
Case2	0	0	0	1
Case3	0	0	3	1
Case4	1	0	3	1
Case5	1	2	3	1

Table 5.2: Predator-prey test cases of different reaction coefficients

CDRE can be utilized. The system of equations reads:

$$\begin{bmatrix}\partial_t u_1\\ \partial_t u_2\end{bmatrix} - \begin{bmatrix}k_1\Delta u_1\\ k_2\Delta u_2\end{bmatrix} + \begin{bmatrix}\mathbf{a}_1\cdot\nabla u_1\\ \mathbf{a}_2\cdot\nabla u_2\end{bmatrix} - \begin{bmatrix}s_{11}(1-u_1) & -s_{12}\dfrac{u_1}{1+\alpha_1 u_1}\\ -s_{21}\dfrac{u_1}{1+\alpha_2 u_1} & s_{22}\end{bmatrix}\begin{bmatrix}u_1\\ u_2\end{bmatrix} = \begin{bmatrix}f_1\\ f_2\end{bmatrix}$$

with suitable initial and boundary conditions (5.10)

In the above equation, $s_{11} = C$, $K = 1$, $s_{12} = \frac{B}{H}$, $\alpha_1 = \frac{1}{H}$, $s_{21} = \frac{\kappa B}{H}$, $\alpha_2 = \frac{1}{H}$ and $s_{22} = -M$.

5.3.2 Numerical tests and results

Let us consider the predator-prey equation within a unit square domain (Eqn 5.11) with initial condition (population density) shown in Fig. 5.11 and boundary conditions. The initial population density is a normal distribution. A number of

cases are run for different values of the reaction coefficients s_{ij} where $i, j = 1:2$. They are indicated in the table 5.2. Other coefficients are retained as constant for all the cases. Diffusion coefficients are $k_1 = k_2 = 10^{-4}$, convection velocity fields are $\mathbf{a}_1 = 0.5\binom{1}{1}$ and $\mathbf{a}_2 = 0.5\binom{-1}{-1}$. Hence predator and prey populations are driven in opposite directions for head-on encounter with one another. No source terms are considered (f_1 and $f_2 = 0$) and constants α_1 and α_2 are taken to be unity. The problem reads:

$$\begin{aligned}
&\begin{bmatrix} \partial_t u_1 \\ \partial_t u_2 \end{bmatrix} - \begin{bmatrix} k_1 \Delta u_1 \\ k_2 \Delta u_2 \end{bmatrix} + \begin{bmatrix} \mathbf{a}_1 \cdot \nabla u_1 \\ \mathbf{a}_2 \cdot \nabla u_2 \end{bmatrix} \\
&- \begin{bmatrix} s_{11}(1-u_1) & -s_{12}\dfrac{u_1}{1+\alpha u_1} \\ -s_{21}\dfrac{u_1}{1+\alpha u_1} & s_{22} \end{bmatrix} \begin{bmatrix} u_1 \\ u_2 \end{bmatrix} = \begin{bmatrix} f_1 \\ f_2 \end{bmatrix} \qquad \text{in } \Omega = [0,1] \times [0,1] \qquad (5.11) \\
&\qquad\qquad u_1(x, y, t > 0) = 0 \qquad \text{on } \partial\Omega \\
&\qquad\qquad u_2(x, y, t > 0) = 0 \qquad \text{on } \partial\Omega
\end{aligned}$$

The domain is discretized with quadrilateral elements with h = 0.02. Hence Pe = 50 and considering the maximum values of s_{11} and s_{22}, Da = 4. The temporal domain $t = [0\ 1]$ and solution snapshots at $t = 0.2, 0.4, 0.6, 0.8, 1.0$ indicated for each case.

5.3.2.1 Case1: $s_{11} = 0, s_{12} = 0, s_{21} = 0$ and $s_{22} = 0$

Case1 represents the absence of reaction terms. Diffusion is relatively weak compared to convection. The equations are uncoupled and independent of each other. In fig 5.12, we can observe a small diffusion and consequently large advection of the population along the direction of the advection velocity. Since there is no interaction, the populations of predator and prey do not affect each other. This case is important to observe the effect of transport and diffusion alone. It will serve as a reference for comparison to cases with reaction terms.

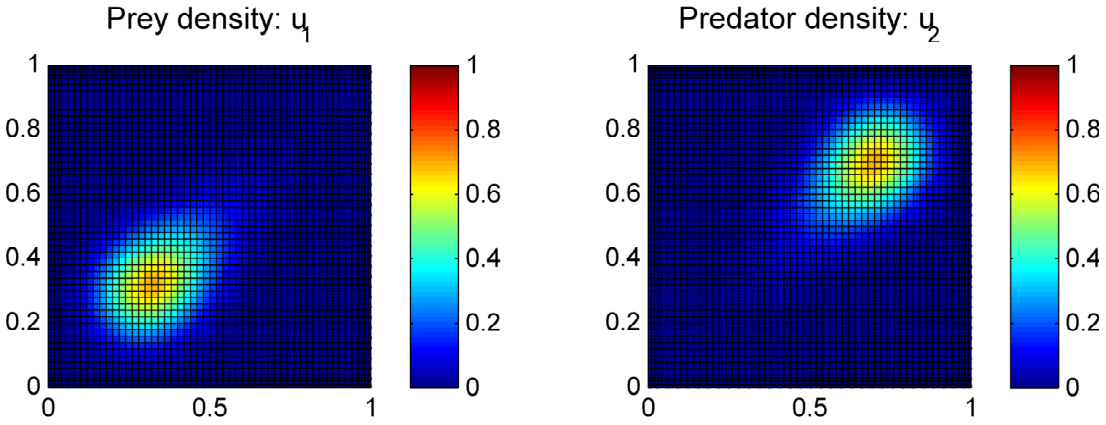

(a) $t = 0.2$

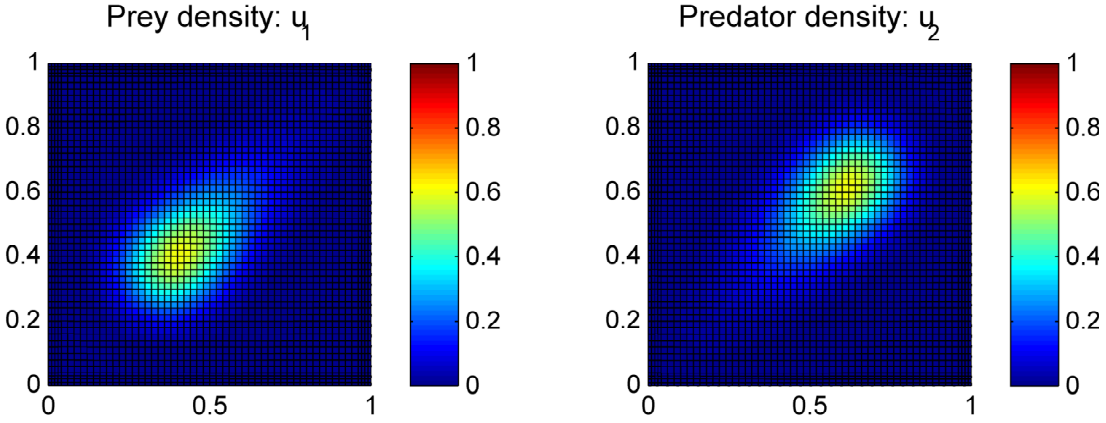

(b) $t = 0.4$

Figure 5.12: Predator-prey population densities for Case1. $s_{11} = 0, s_{12} = 0, s_{21} = 0$ and $s_{22} = 0$

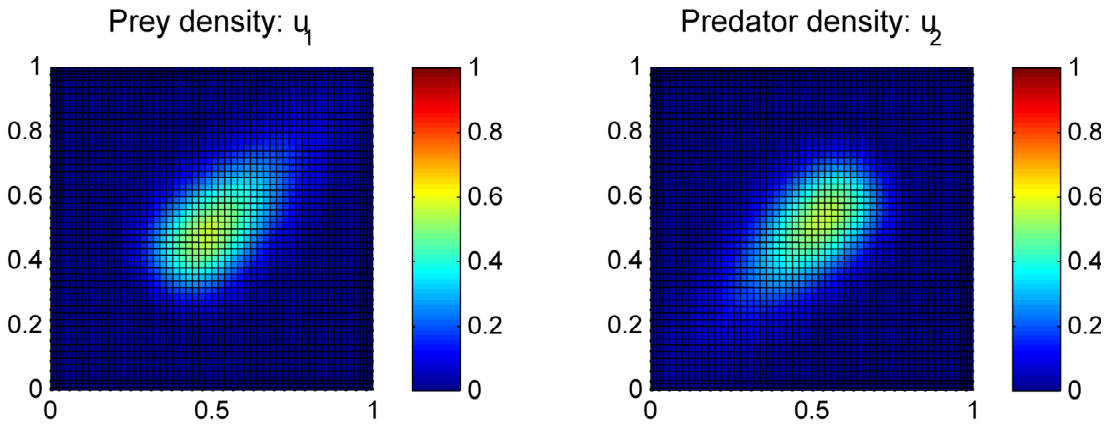

(c) $t = 0.6$

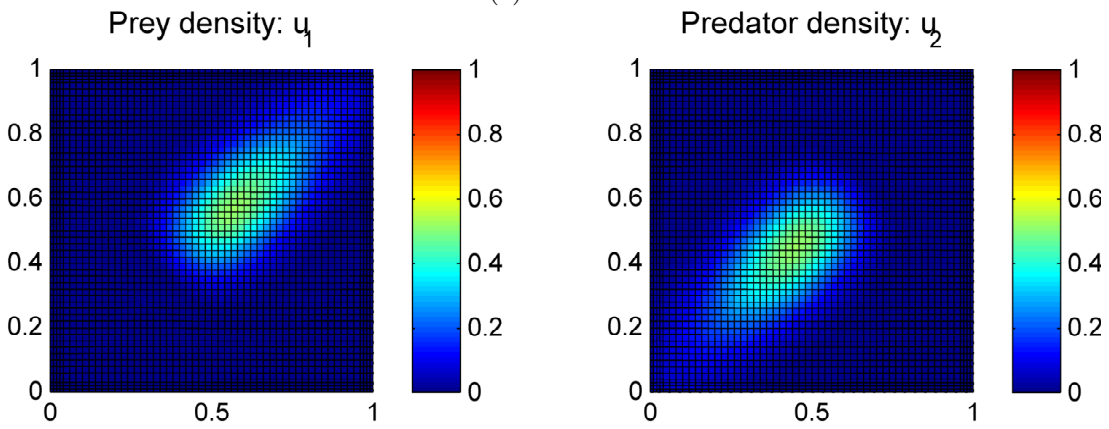

(d) $t = 0.8$

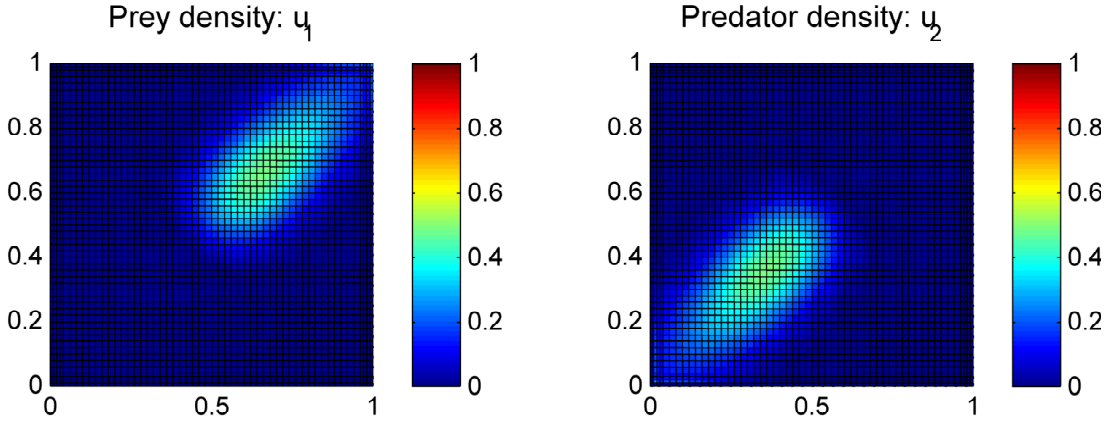

(e) $t = 1.0$

Figure 5.12: Predator-prey population densities for Case1. $s_{11} = 0, s_{12} = 0, s_{21} = 0$ and $s_{22} = 0$

5.3.2.2 Case2: $s_{11} = 0, s_{12} = 0, s_{21} = 0$ and $s_{22} = 1$

In Case2, $s_{22} = 1$. The prey population is still governed by convection-diffusion but the predator is governed by a CDRE with linear reaction. The linear reaction term models the decline of the predator due to lack of availability of prey. Hence we expect a temporal decline of population of predator and we can observe that in fig 5.13. As in Case1, both equations are uncoupled and independent of one another. Hence the solution for the prey remains the same as in Case1.

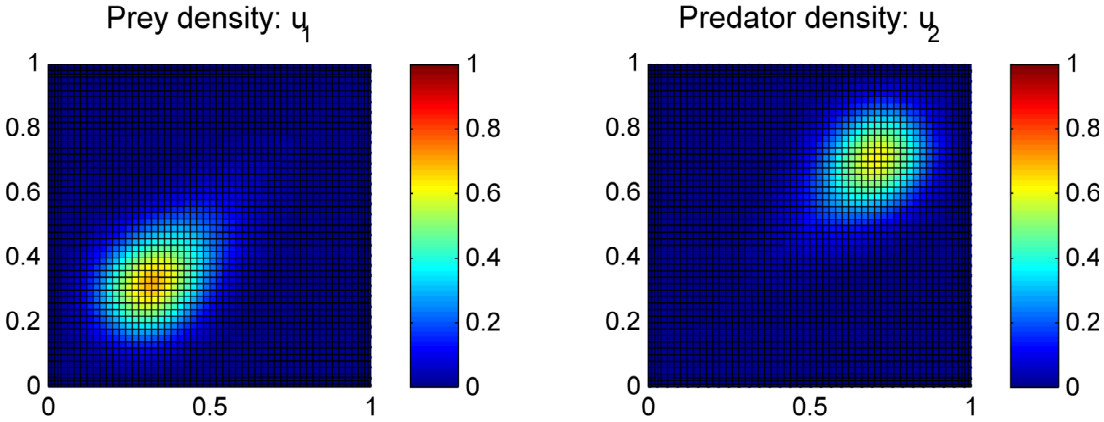

(a) $t = 0.2$

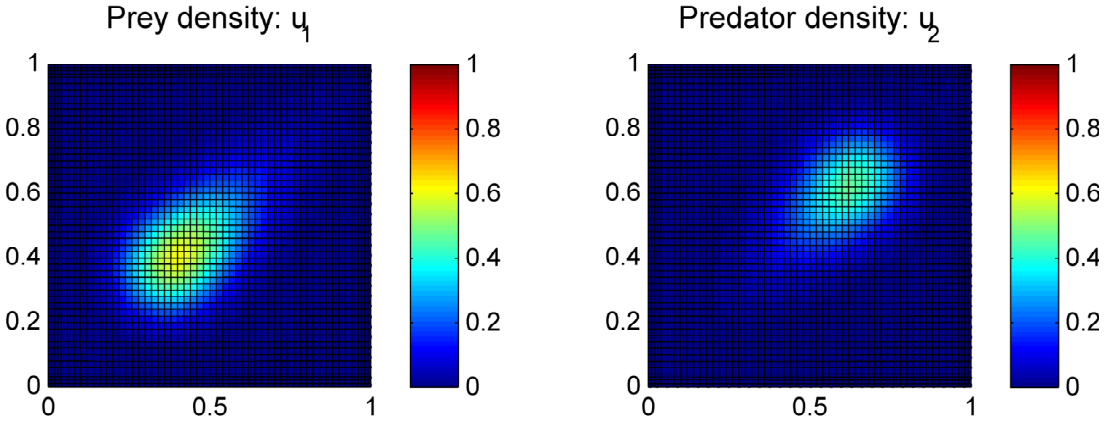

(b) $t = 0.4$

Figure 5.13: Predator-prey population densities for Case2. $s_{11} = 0, s_{12} = 0, s_{21} = 0$ and $s_{22} = 1$

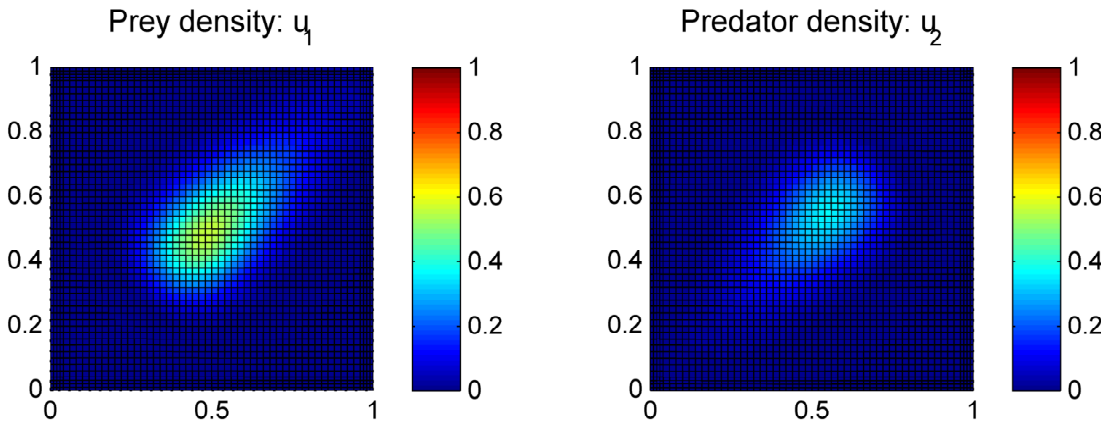

(c) $t = 0.6$

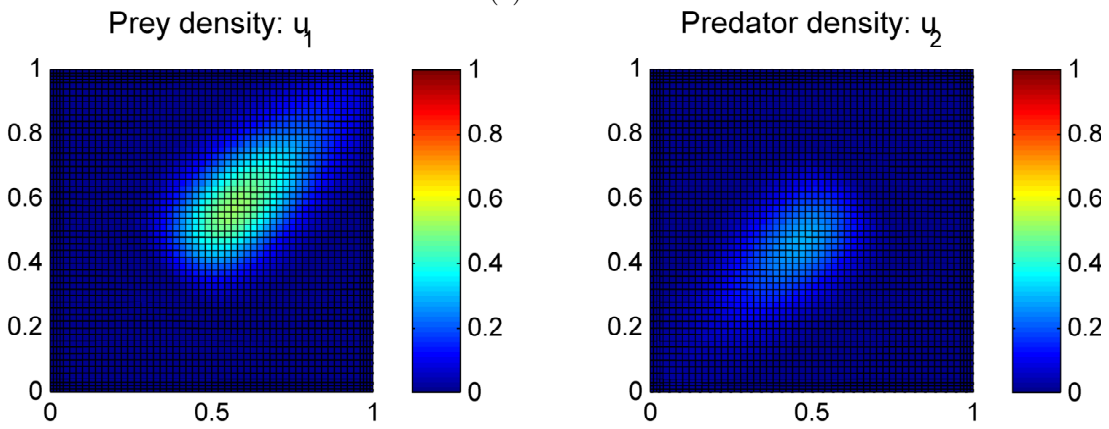

(d) $t = 0.8$

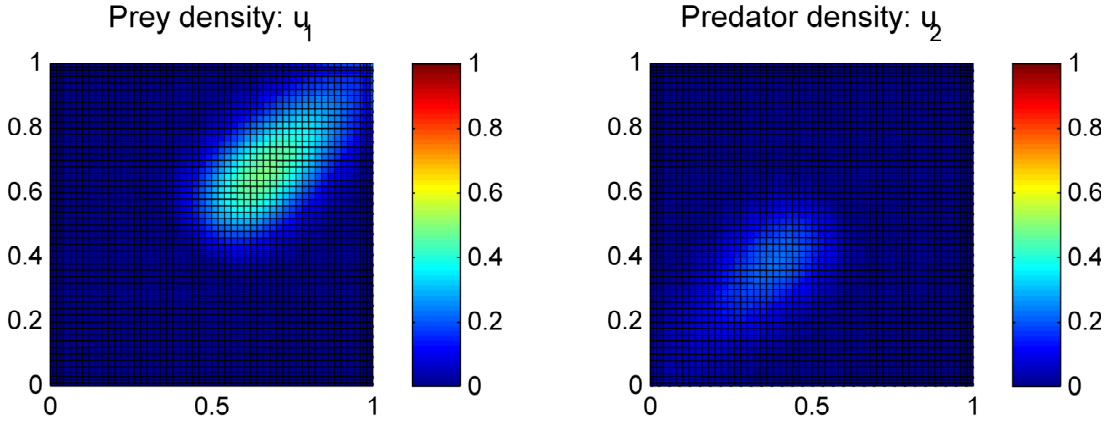

(e) $t = 1.0$

Figure 5.13: Predator-prey population densities for Case2. $s_{11} = 0, s_{12} = 0, s_{21} = 0$ and $s_{22} = 1$

5.3.2.3 Case3: $s_{11} = 0, s_{12} = 0, s_{21} = 3$ and $s_{22} = 1$

Case 3 adds more complexity to the predator equation with s_{22} =1 and $s_{21} = 3$. For the predator, the contribution of decline of species by mortality and growth by predation is added. We can see that it is now linked to the prey population through a one-way coupling (prey population is not affected by predator). This is evident in the fig 5.14. In fig 5.14 (a) and (b), the predator population declines. But after encountering the prey the predator population rapidly increases as depicted in fig 5.14 (c) and (d). In fig 5.14 (e) we observe that predator population declines in the absence of prey.

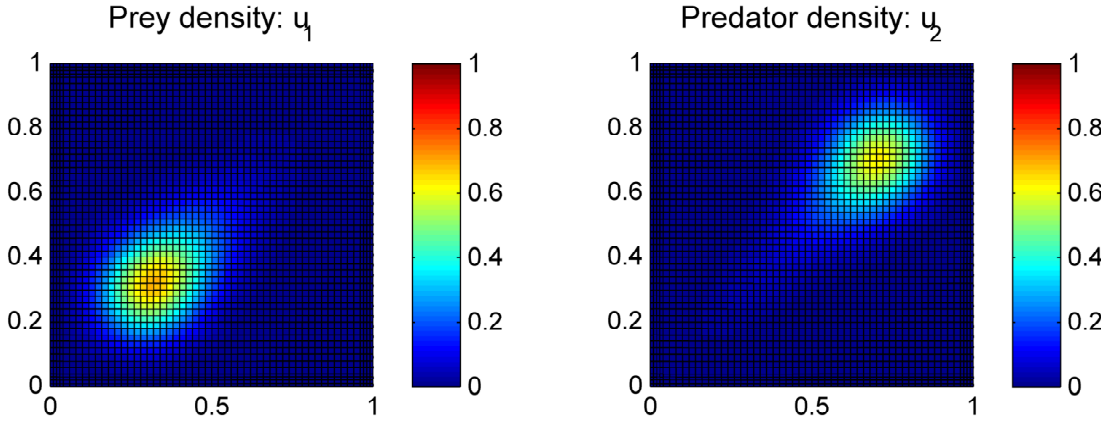

(a) $t = 0.2$

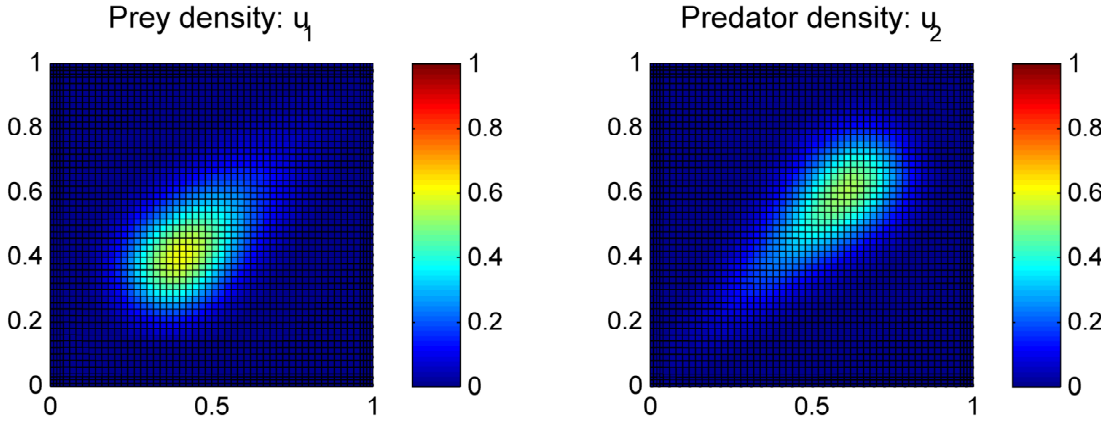

(b) $t = 0.4$

Figure 5.14: Predator-prey population densities for Case3. $s_{11} = 0, s_{12} = 0, s_{21} = 3$ and $s_{22} = 1$

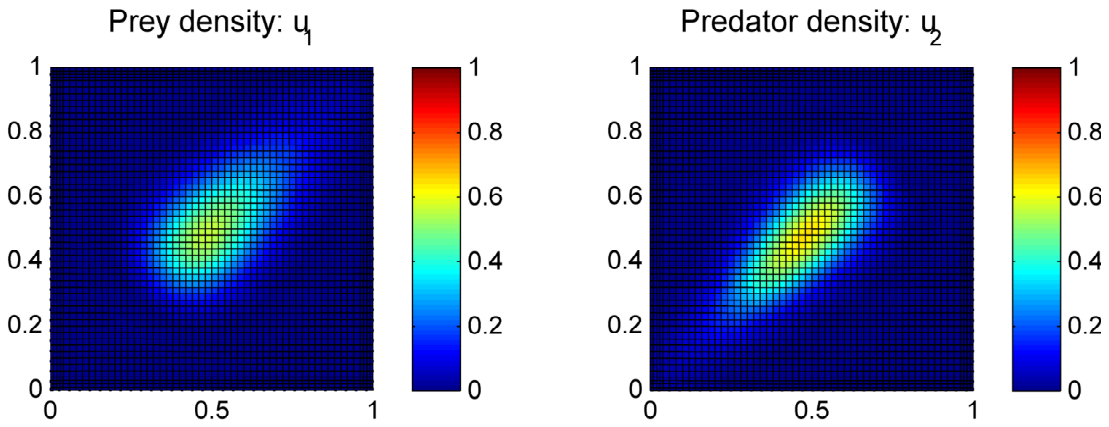

(c) $t = 0.6$

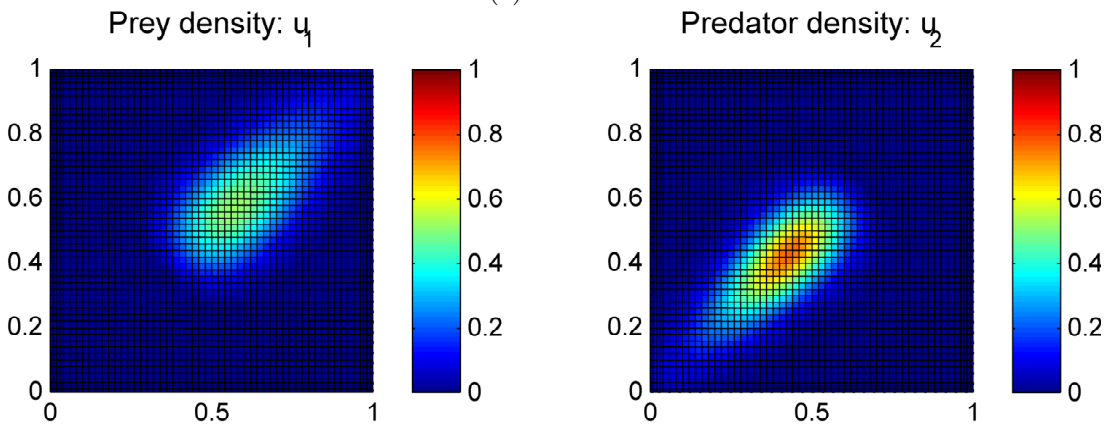

(d) $t = 0.8$

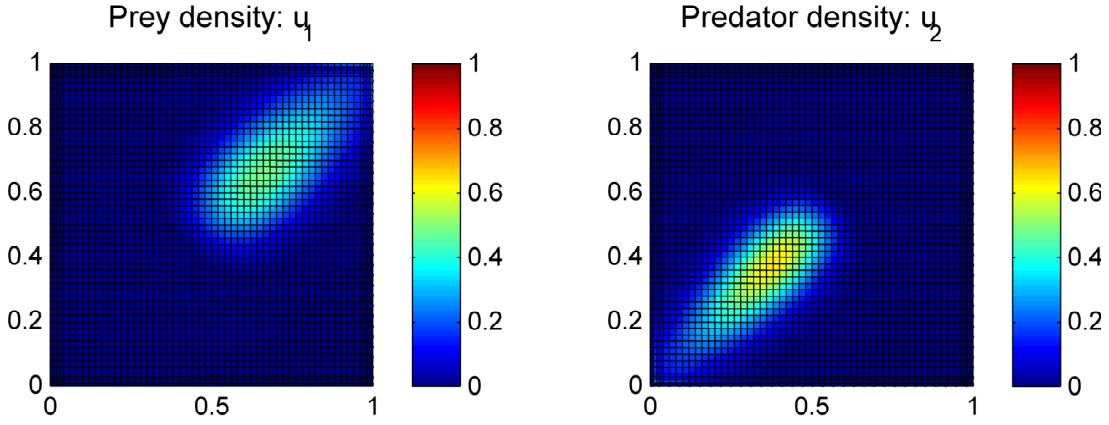

(e) $t = 1.0$

Figure 5.14: Predator-prey population densities for Case3. $s_{11} = 0, s_{12} = 0, s_{21} = 3$ and $s_{22} = 1$

5.3.2.4 Case4: $s_{11} = 1, s_{12} = 0, s_{21} = 3$ and $s_{22} = 1$

Case4 introduces a logistic growth reaction term for the prey population. In this case, along with $s_{22} = 1$ and $s_{21} = 3$, we also have $s_{11} = 1$. We can expect to observe growth in population of prey. But the equations are just one-way coupled. The growth of prey population is indicated in fig 5.15. Due to altered prey population, the dynamics of predator is different too.

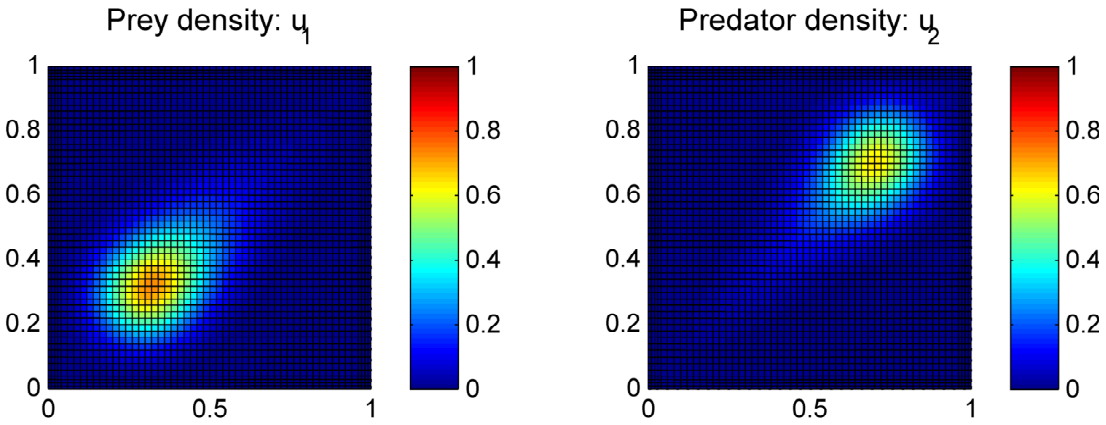

(a) $t = 0.2$

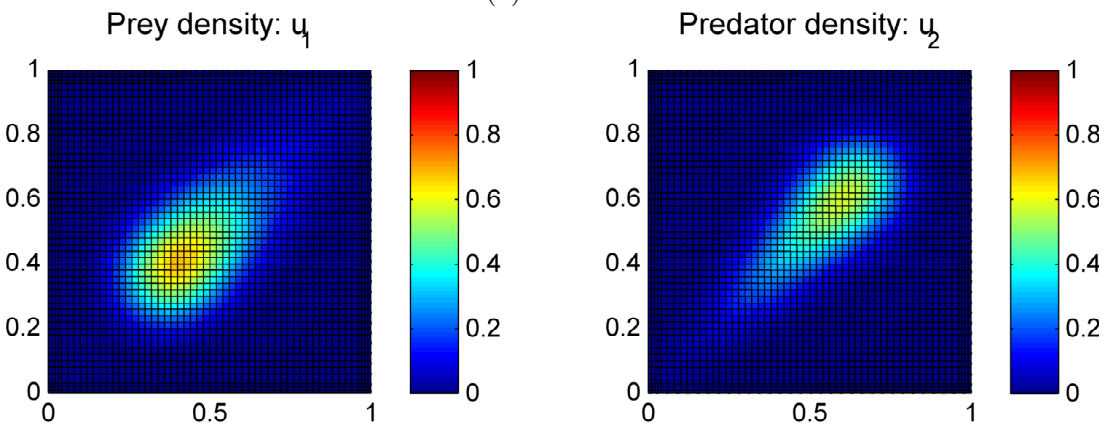

(b) $t = 0.4$

Figure 5.15: Predator-prey population densities for Case4. $s_{11} = 1, s_{12} = 0, s_{21} = 3$ and $s_{22} = 1$

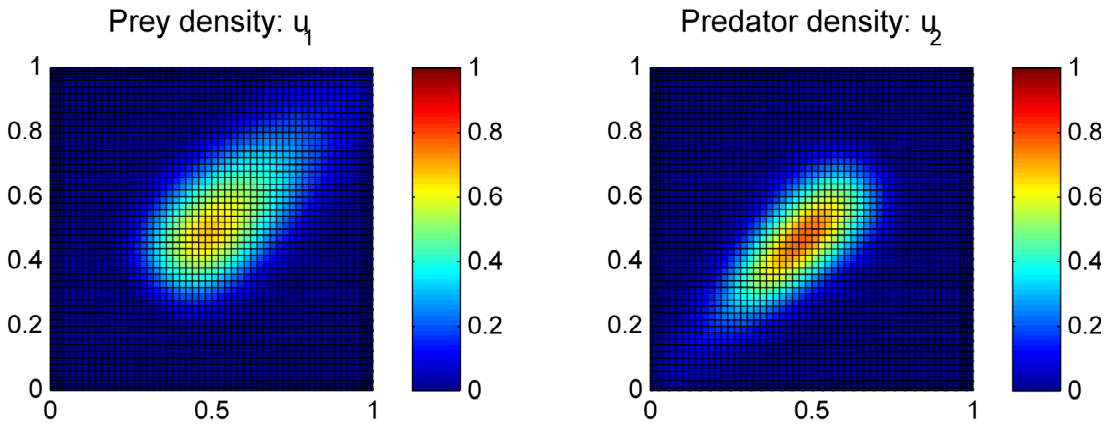

(c) $t = 0.6$

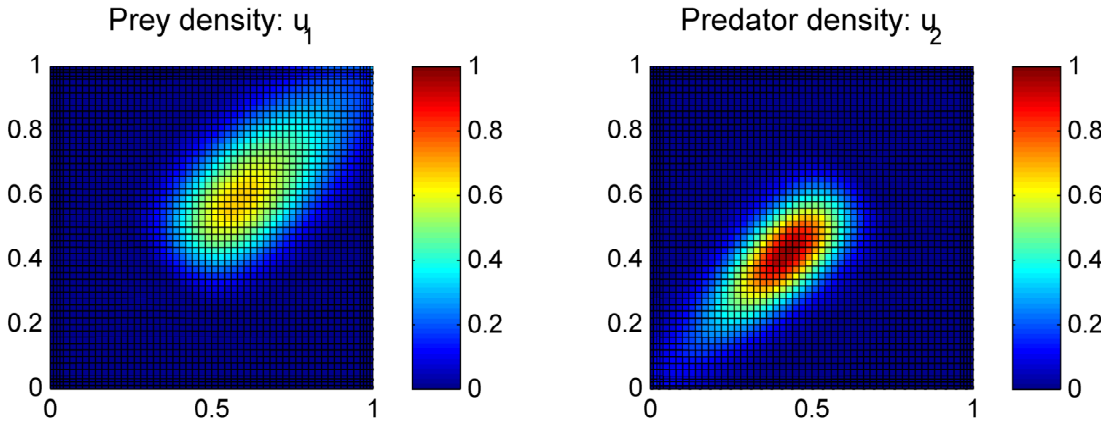

(d) $t = 0.8$

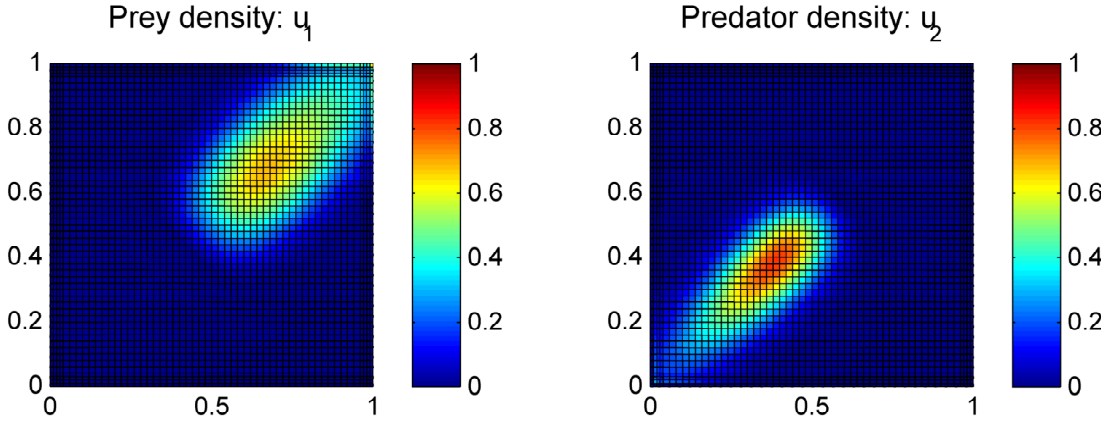

(e) $t = 1.0$

Figure 5.15: Predator-prey population densities for Case4. $s_{11} = 1, s_{12} = 0, s_{21} = 3$ and $s_{22} = 1$

5.3.2.5 Case5: $s_{11} = 1, s_{12} = 2, s_{21} = 3$ and $s_{22} = 1$

Case5 is the most realistic and comprehensive case. Growth and decline of populations of both prey and predator are considered and there is a two-way coupling in the equation. The prey population grows in a logistical manner with mortality by predation. On the other hand, predation fuels the growth of predator and but its mortality controls overpopulation. Predation occurs when both populations meet spacially at the same time. The behaviour is highly nonlinear as seen in fig 5.16. Diffusion, convection and reaction terms compete to produce a net result which interacts with that of the other population. This in-turn affects its own population.

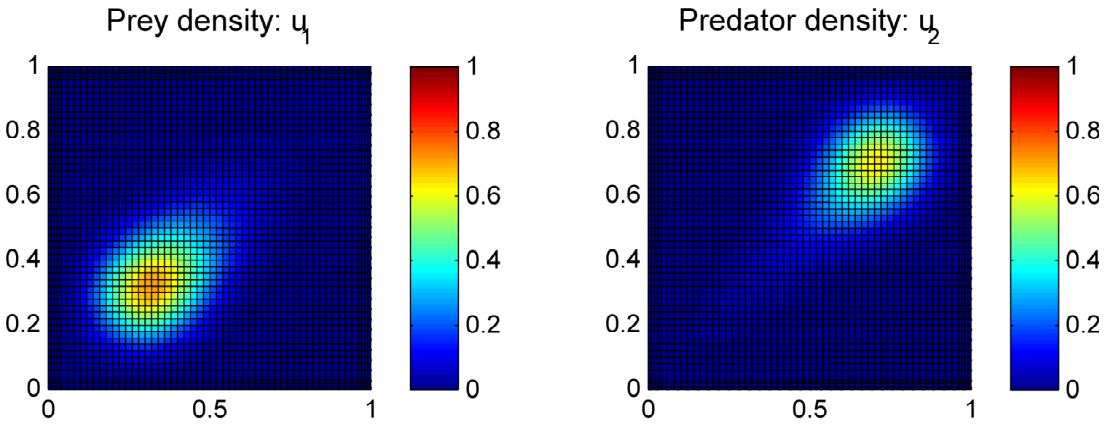

(a) $t = 0.2$

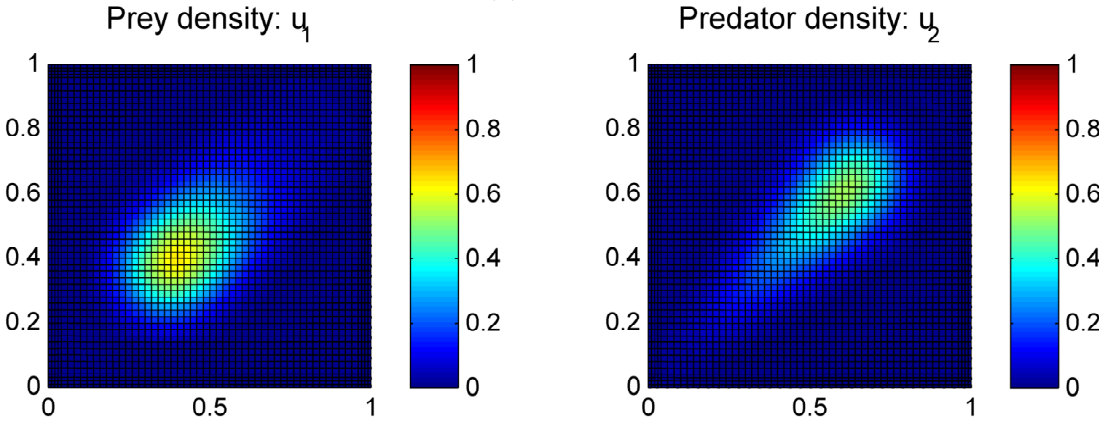

(b) $t = 0.4$

Figure 5.16: Predator-prey population densities for Case5. $s_{11} = 1, s_{12} = 2, s_{21} = 3$ and $s_{22} = 1$

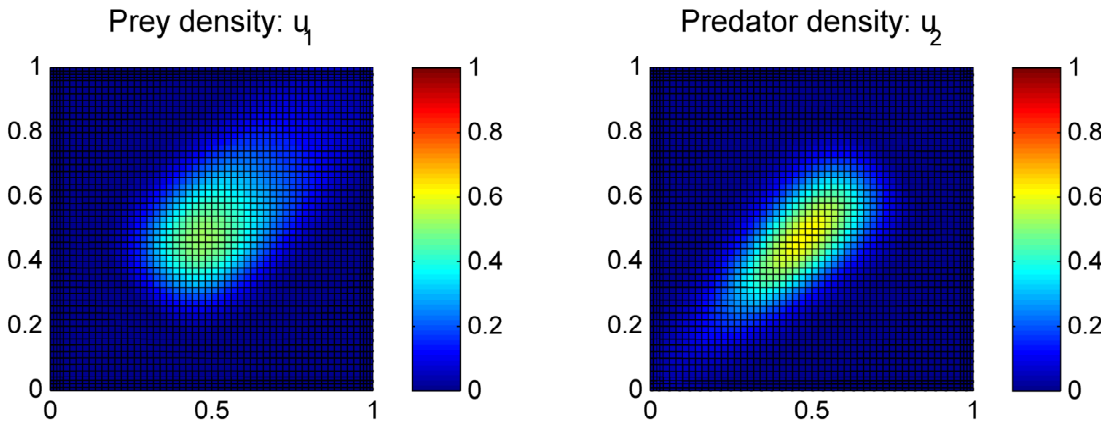

(c) $t = 0.6$

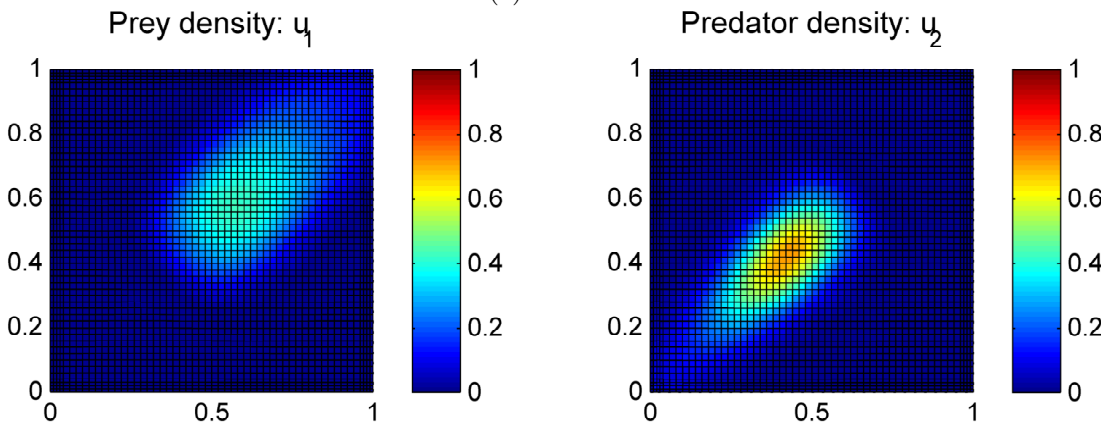

(d) $t = 0.8$

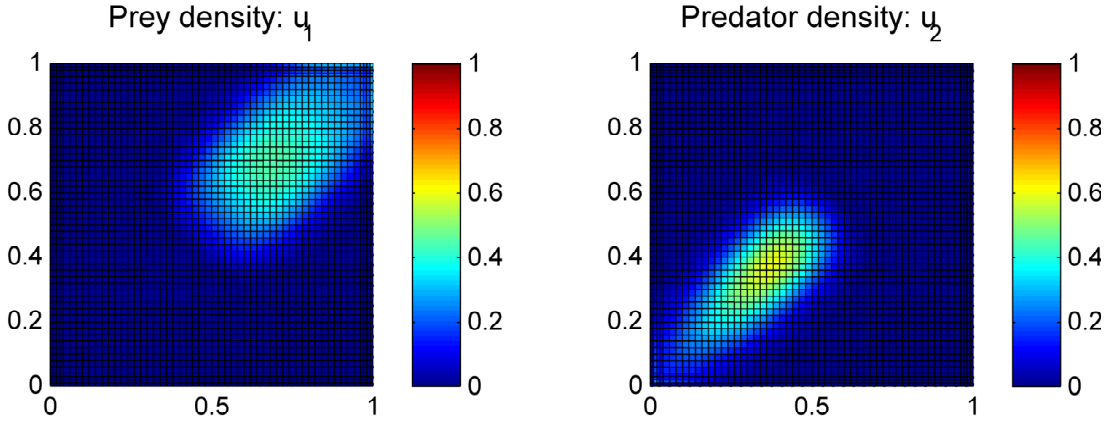

(e) $t = 1.0$

Figure 5.16: Predator-prey population densities for Case5. $s_{11} = 1, s_{12} = 2, s_{21} = 3$ and $s_{22} = 1$

High Pe and Da numbers are observed but OSS stabilization provides control over the error and oscillation-free accurate results are obtained. Fig 5.17 and 5.18 shows the convergence of solution u_1 and u_2 at every time step for each iteration of Newton Raphson linearization. Since the stabilization parameter is constant for all Newton Raphson iteration in a time step, the convergence rate is linear. As pointed out in the previous chapter, this was chosen to save on numerical expenses. If u_{i+1}^{n+1} is the updated solution and u_i^{n+1} is the solution at previous iteration at current time step $n+1$, L^2 norm of error in u is given in Eqn 5.12. Acceptable tolerance for the error was set to 0.1%.

$$\text{Normalized error } = \frac{||u_{i+1}^{n+1} - u_i^{n+1}||_{L^2}}{||u_i^{n+1}||_{L^2}} \tag{5.12}$$

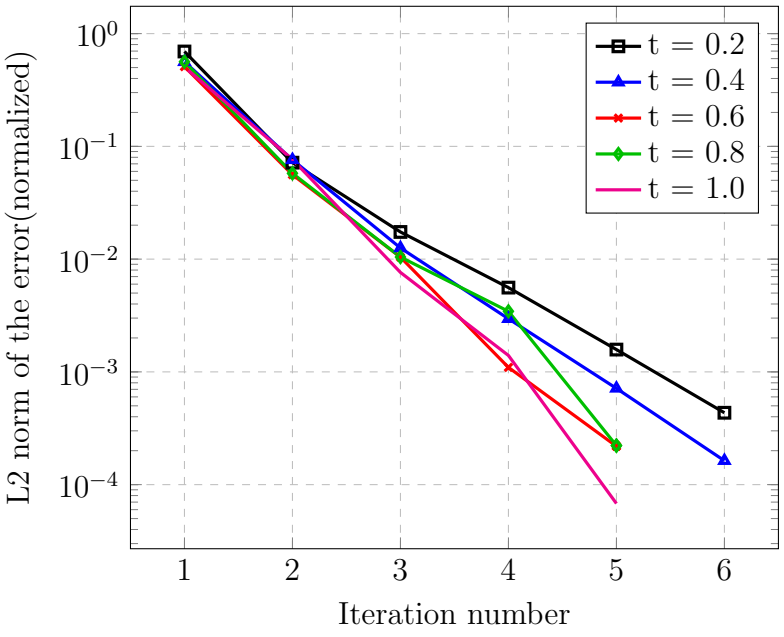

Figure 5.17: Convergence plot for Newton Raphson linearization of u_1

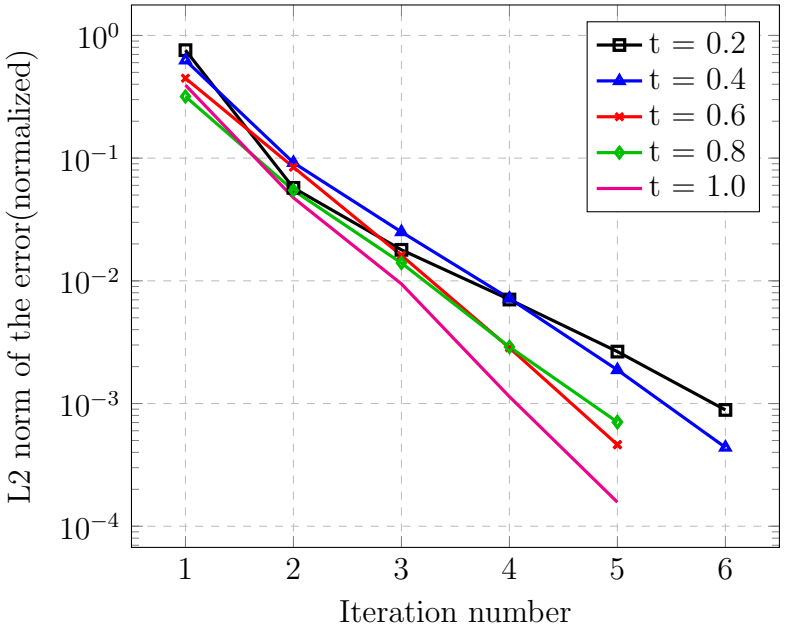

Figure 5.18: Convergence plot for Newton Raphson linearization of u_2

Chapter 6

Conclusion

In the present study, we highlighted the ubiquity of CDRE in modeling of physical phenomenon. Our focus was concentrated upon models with nonlinear reaction term. Such equations arise in population study, circuit theory, quantum mechanics, etc. Solution exhibit varied properties such as pattern formation, periodicity and bifurcation. When considering Fisher-KPP equation, one of the earliest and most widely used CDRE with nonlinear reaction, we noted that obtaining numerical solution isn't straightforward. This was especially true for CDRE with different scales for convection, diffusion and reaction terms. We introduced two non-dimensional quantities. Numerical Peclet number Pe is a measure of relative strength of convection to that of diffusion and numerical Damköhler number Da is a measure of relative strength of reaction to that of diffusion. When Pe and Da are large, Galerkin finite element method does not yield stable and smooth solution. This inspired us to utilize stabilization techniques which became the main objective of our study.

Our preferred choice of stabilization is Orthogonal Subgrid Scale method which is a derivative of Variational Multi Scale approach. The key idea is the decomposition of unknown solution into a finite element resolvable component and unresolvable component. The former was referred to as coarse grid and the latter as the fine grid component in VMS terminology. When it comes to approximating the fine grid component, OSS methodology utilizes the property that if the sum decomposition formulation is to represent a highly accurate solution, the error in the coarse grid component must be compensated by the fine grid component. In

particular, the choice of functional space for the fine grid component was to be orthogonal to the finite element functional space. And the approximation of the fine grid component was taken to be the L^2 projection onto a space orthogonal to the finite element functional space of the finite element residual. This formulation has the advantage that it is not overly diffusive compared to other stabilization techniques. Moreover, it helps to regain control over the finite element error. But the error is globally bounded and local oscillations in the region of sharp layers were still encountered. This was mitigated by restricting severe oscillations to only few elements using selective mesh refinement. In the end, this formulation led to an additional term to the Galerkin finite element weak form. We presented the exposition of the formulation suitable for CDRE and implementation was detailed.

First implementation was for a stationary, linear CDRE. Later, CDRE with nonlinear reaction was implemented. In order to deal with nonlinear terms, we resorted to Newton Raphson linearization. This technique served our purpose fairly well with only a few hiccups for highly nonlinear cases. Since all real-world models for nonlinear CDRE were transient equations, time integration was necessary. Hence an implementation of Backward Differences scheme was included. The OSS stabilization term was constant for each time step and was independent of temporal terms. Implementation was extended to include coupled system of CDREs.

Next step was the testing phase. The implementation was checked for correctness and tests were necessary to ensure that they were bug-free. The choice was to use method of manufactured solutions to test the implementation. Convergence study for error was carried out for all implementations. One could observe optimal convergence rates and this instill confidence in our implementation. The code was ready to solve real-world applications.

We set out to demonstrate the advantages of OSS stabilization via solving real-world problems. The first example was the solution of CDRE in a channel flow. This case presented a scenario where the stabilization was successful in obtaining a smooth solution for moderately large advection and reaction phenomenon. When very large Pe and Da numbers were encountered, complex physics was unable to be resolved with the current linearization technique. This highlighted the

advantages and shortcomings of the method employed. Cavity flow was the next example which presented a complex advection field. The method was able to successfully generate a stable solution and sharp layers were captured. We saw that small efforts at performing selective refinement could yield great benefits in terms of reduction of local oscillations and accurate representation of transition zone. The next problem that was tackled was a predator-prey model consisting of coupled transient nonlinear system of CDREs. This dynamical system was solved for various test scenarios and we could capture the complex interaction for large Pe and Da numbers.

We conclude that stabilization is necessary for finite element solution of nonlinear CDRE for large Pe and Da numbers. In particular, OSS offered good stability and globally smooth solution with least added numerical diffusion. The problem with local oscillations was mitigated with selective mesh refinement. Sharp layers in the solution were captured well without oscillations. Newton Raphson method was the preferred choice for linearization of nonlinear reaction terms. Application of the formulation to various examples highlighted the strengths and limitations of this choice of linearization. Newton Rapshon is a robust scheme but falters when nonlinearity is very large and sudden (for which the initial guess is not close enough for the scheme to converge). With respect to the error analysis, we observed optimal convergence behaviour in our numerical tests of our implementation. Method of manufactured solutions was utilized and this validated the correctness of our implementation. Three examples of real-world problems were solved which extol the benefits of OSS stabilization.

Several possible research avenues branch out from this study. The formulation can be applied to large systems such as air pollution monitoring, contaminant dispersal in marine environments using real-world data. Rewarding insights can be reaped by tackling challenges of such large scale systems. Different linearization techniques in conjunction with OSS stabilized finite element formulation could be tested to study the pros and cons of each scheme. This can act as a reference for scenarios where a choice needs to be made. Nonlinearity in diffusion and convection terms could be introduced which opens up more applications for the formulation. A two way coupling with a flow solver could be implemented.

References

Donald G Aronson and Hans F Weinberger. Nonlinear diffusion in population genetics, combustion, and nerve pulse propagation. In *Partial differential equations and related topics*, pages 5–49. Springer, 1975. 4

Ramon Codina; Javier Principe; Joan Baiges. Subscales on the element boundaries in the variational two-scale finite element method. *Computer Methods in Applied Mechanics and Engineering*, 198, 2009. doi: 10.1016/j.cma.2008.10.020. URL http://gen.lib.rus.ec/scimag/index.php?s=10.1016/j.cma.2008.10.020. 10

M. Bär and M. Eiswirth. Turbulence due to spiral breakup in a continuous excitable medium. *Phys. Rev. E*, 48:R1635–R1637, Sep 1993. doi: 10.1103/PhysRevE.48.R1635. URL http://link.aps.org/doi/10.1103/PhysRevE.48.R1635. 4

Javier Principe; Ramon Codina. On the stabilization parameter in the subgrid scale approximation of scalar convectiondiffusionreaction equations on distorted meshes. *Computer Methods in Applied Mechanics and Engineering*, 199, 2010. doi: 10.1016/j.cma.2009.08.011. URL http://gen.lib.rus.ec/scimag/index.php?s=10.1016/j.cma.2009.08.011. 10

Ramon Codina. Comparison of some finite element methods for solving the diffusion-convection-reaction equation. *Computer Methods in Applied Mechanics and Engineering*, 156(14):185 – 210, 1998. ISSN 0045-7825. doi: http://dx.doi.org/10.1016/S0045-7825(97)00206-5. URL http://www.sciencedirect.com/science/article/pii/S0045782597002065. 8, 10

Ramon Codina. Stabilized finite element approximation of transient incompressible flows using orthogonal subscales. *Computer Methods in Applied Mechanics and Engineering*, 191(3940):4295 – 4321, 2002. ISSN 0045-7825. doi: http://dx.doi.org/10.1016/S0045-7825(02)00337-7. URL http://www.sciencedirect.com/science/article/pii/S0045782502003377. 5

Ramon Codina and Jordi Blasco. Analysis of a stabilized finite element approximation of the transient convection-diffusion-reaction equation using orthogonal subscales. *Computing and Visualization in Science*, 4(3):167–174, 2002. ISSN 1433-0369. doi: 10.1007/s007910100068. URL http://dx.doi.org/10.1007/s007910100068. 7

E.L. Cussler. *Multicomponent Diffusion*. Chemical Engineering Monographs; V. 3. Elsevier Science, 2013. ISBN 9781483102009. URL https://books.google.es/books?id=C8H8BAAAQBAJ. 1, 2, 3

V.G. Danilov, V.P. Maslov, and K.A. Volosov. *Mathematical Modelling of Heat and Mass Transfer Processes*. Mathematics and Its Applications. Springer Netherlands, 2012. ISBN 9789401104098. URL https://books.google.es/books?id=8QHoCAAAQBAJ. 1

R. A. Fisher. The wave of advance of advantageous genes. *Annals of Eugenics*, 7(4):355–369, jun 1937. doi: 10.1111/j.1469-1809.1937.tb02153.x. URL http://dx.doi.org/10.1111/j.1469-1809.1937.tb02153.x. 1, 3, 4

E. P. Gross. Structure of a quantized vortex in boson systems. *Il Nuovo Cimento (1955-1965)*, 20(3):454–477, 1961. ISSN 1827-6121. doi: 10.1007/BF02731494. URL http://dx.doi.org/10.1007/BF02731494. 4

A. El Hamidi, M. Garbey, and N. Ali. On nonlinear coupled diffusions in competition systems. *Nonlinear Analysis: Real World Applications*, 13(3):1306 – 1318, 2012. ISSN 1468-1218. doi: http://dx.doi.org/10.1016/j.nonrwa.2011.10.007. URL http://www.sciencedirect.com/science/article/pii/S1468121811003014. 1

Matt Holzer. Anomalous spreading in a system of coupled fisherkpp equations. *Physica D: Nonlinear Phenomena*, 270:1 – 10, 2014. ISSN 0167-2789. doi: http://dx.doi.org/10.1016/j.physd.2013.12.003. URL http://www.sciencedirect.com/science/article/pii/S0167278913003308. 1

Thomas J.R. Hughes. Multiscale phenomena: Green's functions, the dirichlet-to-neumann formulation, subgrid scale models, bubbles and the origins of stabilized methods. *Computer Methods in Applied Mechanics and Engineering*, 127(14):387 – 401, 1995. ISSN 0045-7825. doi: http://dx.doi.org/10.1016/0045-7825(95)00844-9. URL http://www.sciencedirect.com/science/article/pii/0045782595008449. 5, 8

Thomas J.R. Hughes, Gonzalo R. Feijo, Luca Mazzei, and Jean-Baptiste Quincy. The variational multiscale methoda paradigm for computational mechanics. *Computer Methods in Applied Mechanics and Engineering*, 166 (12):3 – 24, 1998. ISSN 0045-7825. doi: http://dx.doi.org/10.1016/S0045-7825(98)00079-6. URL http://www.sciencedirect.com/science/article/pii/S0045782598000796. Advances in Stabilized Methods in Computational Mechanics. 8

B. Linares-Barranco, E. Sanchez-Sinencio, A. Rodriguez-Vazquez, and J. L. Huertas. A cmos implementation of fitzhugh-nagumo neuron model. *IEEE Journal of Solid-State Circuits*, 26(7):956–965, Jul 1991. ISSN 0018-9200. doi: 10.1109/4.92015. 2

Eugen Magyari. Exact analytical solution of a nonlinear reactiondiffusion model in porous catalysts. *Chemical Engineering Journal*, 143(13):167 – 171, 2008. ISSN 1385-8947. doi: http://dx.doi.org/10.1016/j.cej.2008.03.018. URL http://www.sciencedirect.com/science/article/pii/S1385894708001800. 5

Horst Malchow. *Spatiotemporal patterns in ecology and epidemiology : theory, models, and simulation*. Chapman & Hall/CRC Press, Boca Raton, 2008. ISBN 9781584886747. 46

J. Nagumo, S. Arimoto, and S. Yoshizawa. An active pulse transmission line

simulating nerve axon. *Proceedings of the IRE*, 50(10):2061–2070, Oct 1962. ISSN 0096-8390. doi: 10.1109/JRPROC.1962.288235. 2, 4

C.V Pao. On nonlinear reaction-diffusion systems. *Journal of Mathematical Analysis and Applications*, 87(1):165 – 198, 1982. ISSN 0022-247X. doi: http://dx.doi.org/10.1016/0022-247X(82)90160-3. URL http://www.sciencedirect.com/science/article/pii/0022247X82901603. 4

S. Tang and R. O. Weber. Numerical study of fisher's equation by a petrov-galerkin finite element method. *The Journal of the Australian Mathematical Society. Series B. Applied Mathematics*, 33:27–38, 7 1991. ISSN 1446-8735. doi: 10.1017/S0334270000008602. URL http://journals.cambridge.org/article_S0334270000008602. 5

V.M. Tikhomirov. *Selected Works of A. N. Kolmogorov: Volume I: Mathematics and Mechanics*. Mathematics and its Applications. Springer Netherlands, 1991. ISBN 9789027727961. URL https://books.google.es/books?id=ikN59GkYJKIC. 3, 4

A. M. Turing. The chemical basis of morphogenesis. *Philosophical Transactions of the Royal Society B: Biological Sciences*, 237(641):37–72, aug 1952. doi: 10.1098/rstb.1952.0012. URL http://dx.doi.org/10.1098/rstb.1952.0012. 4

V. Volpert and S. Petrovskii. Reactiondiffusion waves in biology. *Physics of Life Reviews*, 6(4):267 – 310, 2009. ISSN 1571-0645. doi: http://dx.doi.org/10.1016/j.plrev.2009.10.002. URL http://www.sciencedirect.com/science/article/pii/S1571064509000347. 4, 5

Dongmei Zhang, Lszl Gyrgyi, and William R. Peltier. Deterministic chaos in the belousovzhabotinsky reaction: Experiments and simulations. *Chaos*, 3(4):723–745, 1993. doi: http://dx.doi.org/10.1063/1.165933. URL http://scitation.aip.org/content/aip/journal/chaos/3/4/10.1063/1.165933. 4

Jiansong Zhang, Jiang Zhu, and Rongpei Zhang. Characteristic splitting mixed finite element analysis of keller–segel chemotaxis models. *Applied Mathematics and Computation*, 278:33–44, mar 2016. doi: 10.1016/j.amc.2016.01.021. URL http://dx.doi.org/10.1016/j.amc.2016.01.021. 1

Linhe Zhu, Hongyong Zhao, and Haiyan Wang. Complex dynamic behavior of a rumor propagation model with spatial-temporal diffusion terms. *Information Sciences*, 349-350:119–136, jul 2016. doi: 10.1016/j.ins.2016.02.031. URL http://dx.doi.org/10.1016/j.ins.2016.02.031. 2